VŠB - Technická univerzita Ostrava
Fakulta strojní
Katedra mechaniky

Flow Visualization in Surrounding of Aircraft Fuselage

Vizualizace proudění v okolí trupu letadla

Student: Jana Przeczková
Vedoucí bakalářské práce(supervisor): Ing.Zdeněk Poruba, Ph.D
Dr.Tom Scanlon

Ostrava 2010

VŠB - Technická univerzita Ostrava
Fakulta strojní
Katedra mechaniky

Zadání bakalářské práce

Student: **Jana Przeczková**

Studijní program: B2341 Strojírenství

Studijní obor: 3901R003 Aplikovaná mechanika

Téma: Vizualizace proudění v okolí trupu dopravního letadla
Flow Visualization in Surrounding of Aircraft Fuselage

Zásady pro vypracování:

1) Uveďte a popište základní vztahy pro matematický popis proudění.
2) Poskytnutý geometrický model dopravního letadla upravte pro použití ve výpočetním softwarovém balíku Ansys Workbench.
3) Na základě geometrického modelu vytvořte vhodný CFD model oblasti, ve které bude proudění uvažováno, diskutujte možnost použití okrajových podmínek z hlediska možného zjednodušení modelu.
4) Proveďte výpočet a vizualizujte proudění pro 3 různé sklony trupu letadla a další zadané okrajové podmínky.
5) Diskutujte další možnosti využití vytvořeného modelu, např. pro vizualizaci rozložení tlakového pole v okolí trupu letadla.

Seznam doporučené odborné literatury:

[1] RODI, W., FUEYO, N. *Engineering Turbulence Modelling and Experiments 5*. 1st edition. Oxford : Elsevier, 2002. 1010 s. ISBN 0-08-044114-9.
[2] PORUBA, Z., SZWEDA, J. Flow Problem in Thermal Motor Analysis. *Sborník vědeckých prací Vysoké školy báňské – Technické univerzity Ostrava : Řada strojní* [online]. 2008, vol. 54, no. 2 [cit. 2009-11-10], s. 109-114. ISSN 1210-0471.
[3] *ANSYS, Inc. Theory Reference* [online]. 2004 [cit. 2009-11-01]. Dostupný z WWW: <http://www1.ansys.com/customer/content/documentation/90/ansys/a_thry90.pdf>.

Formální náležitosti a rozsah bakalářské práce stanoví pokyny pro vypracování zveřejněné na webových stránkách fakulty.

Vedoucí bakalářské práce: **Ing. Zdeněk Poruba, Ph.D.**

Datum zadání: 10.11.2009

Datum odevzdání: 21.05.2010

VYSOKÁ ŠKOLA BÁŇSKO-TECHNICKÁ UNIVERZITA FAKULTA STROJNÍ 5 OSTRAVA

doc. Ing. Jiří Podešva, Ph.D.
vedoucí katedry

prof. Ing. Radim Farana, CSc.
děkan fakulty

Na tomto místě bych ráda poděkovala mému supervisorovi Dr.Tomu Scanlonovi z University of Strathclyde, Glasgow, bez jehož rad a pomoci by bylo obtížné bakalářskou práci vypracovat.

I would like to thank my supervisor Dr. Tom Scanlon from the University of Strathclyde, Glasgow, without whose help and advice I would not have been able to complete my Bachelor thesis.

Prohlášení studenta

Prohlašuji, že jsem celou bakalářskou práci včetně příloh vypracovala samostatně pod vedením vedoucích bakalářské práce a uvedla jsem všechny použité podklady a literaturu.

V Ostravě ..... podpis studenta .....

Prohlašuji, že

• byla jsem seznámena s tím, že na moji bakalářskou práci se plně vztahuje zákon č. 121/2000 Sb., autorský zákon, zejména §35 – užití díla v rámci občanských a náboženských obřadů, v rámci školních představení a užití díla školního a §60 – školní dílo.

• beru na vědomí, že Vysoká škola báňská – Technická univerzita Ostrava (dále jen VŠB-TUO) má právo nevýdělečně ke své vnitřní potřebě bakalářskou práci užít (§35 odst. 3).

• souhlasím s tím, že jeden výtisk bakalářské práce bude uložen v Ústřední knihovně VŠB-TUO k prezenčnímu nahlédnutí a jeden výtisk bude uložen u vedoucího bakalářské práce. Souhlasím s tím, že údaje o bakalářské práci budou zveřejněny v informačním systému VŠB-TUO.

• bylo sjednáno, že s VŠB-TUO, v případě zájmu z její strany, uzavřu licenční smlouvu s oprávněním užít dílo v rozsahu §12 odst. 4 autorského zákona.

• bylo sjednáno, že užít své dílo – bakalářskou práci nebo poskytnout licenci k jejímu využití mohu jen se souhlasem VŠB-TUO, která je oprávněna v takovém případě ode mne požadovat přiměřený příspěvek na úhradu nákladů, které byly VŠB-TUO na vytvoření díla vynaloženy (až do jejich skutečné výše).

• beru na vědomí, že odevzdáním své práce souhlasím se zveřejněním své práce podle zákona č.111/1998 Sb., o vysokých školách a o změně a doplnění dalších zákonů (zákon o vysokých školách), ve znění pozdějších předpisů, bez ohledu na výsledek její obhajoby.

V Ostravě: .....

…….

podpis

Jméno a příjmení autora práce: Jana Przeczková

Adresa trvalého pobytu autora práce: Kolmá 502, Šenov

ANOTACE BAKALÁŘSKÉ PRÁCE

PRZECZKOVÁ, J. *Vizualizace proudění v okolí trupu letadla: Bakalářská práce.* VŠB-Technická Univerzita Ostrava, Fakulta strojní, Katedra mechaniky, 2010, 69 s. Vedoucí práce: Ing.Zdeněk Poruba, Ph.D., Dr.Tom Scanlon

Bakalářská práce se zabývá aplikací počítačové dynamiky tekutin na proudění v okolí trupu letadla. Nejprve je uvedena teorie týkající se turbulentního proudění a turbulentních modelů. Poté je provedena vizualizace proudění v okolí trupu letadla a jsou popsány jevy k nimž při tomto proudění dochází.

ANNOTATION OF BACHELOR THESIS

PRZECZKOVÁ, J. *Flow Visualization in Surrounding of Aircraft Fusel*age: *Bachelor thesis.* VŠB-Technical University of Ostrava, Faculty of Mechanical Engineering, Department of Mechanics, 2010, 69 p. Thesis head: Ing.Zdeněk Poruba, Ph.D., Dr.Tom Scanlon

Bachelor thesis is dealing with application of the computational fluid dynamics to the flow in surrounding of aircraft fuselage. The theory of turbulent flow and turbulence models are introduced. The visualization of the flow around the aircraft is modeled and important phenomena occurring in the fluid flow are described.

Contents

Nomenclature

List of abbreviations

A	area
ASM	algebraic stress model
CM	control mass
CV	control volume
CFD	computational fluid dynamics
DSMC	direct simulation Monte Carlo
FDM	finite difference method
FEM	finite element method
FVM	finite volume method
RNG	renormalization group
RSM	Reynolds stress equation models
SST	shear stress transport
3D	three dimensional

List of symbols

Roman symbols

Note: Symbol with not given dimension represents general variable

A	matrix of coefficients	
a_∞	speed of sound	[ms^{-1}]
B	additive constant	[1]
$C_{1\varepsilon}$	model coefficient (k-ε model)	[1]
$C_{2\varepsilon}$	model coefficient (k-ε model)	[1]
C_μ	model coefficient (k-ε model)	[1]
C_D	drag coefficient	[1]
C_L	lift coefficient	[1]
D_F	drag force	[$kgms^{-2}$]
E	total energy	[kgm^2s^{-2}]

$E*$	additive constant	[1]
F_1	blending function	
F_2	blending function	
$\vec{f}$	force vector	[kgms^{-2}]
i	internal energy	[kgm^{2}s^{-2}]
k	kinetic energy	[kgm^{2}s^{-2}]
k'	heat transfer coefficient	[kgs^{-3}K^{-1}]
l	length scale	[m]
L	characteristic length	[m]
$L*$	main dimension at the inlet	[m]
L_F	lift force	[kgms^{-2}]
m	mass	[kg]
Ma	Mach number	[1]
$\vec{n}$	normal vector	
p	pressure	[kgm^{-1}s^{-2}]
P_{ij}	production term	
Re	Reynolds number	[1]
Q	vector of source terms	
S_E	source of energy	[kgm^{2}s^{-2}]
S_{Mi}	momentum source term	
S_{ij}	mean strain rate	
S_ϕ	source term	
S_Φ	time averaged source term	
T	temperature	[K]
Δt	small interval of time	[s]
T_i	turbulence intensity	[1,%]
t	time	[s]
u	velocity component in x direction	[ms^{-1}]
$\vec{u}$	velocity vector	[ms^{-1}]
$\overline{u}_{FS}$	free stream velocity	[ms^{-1}]
$u+$	dimensionless velocity	[1]
u_i	velocity components	[ms^{-1}]

u_j	velocity components	[ms^{-1}]
$\overline{u}_{\max}$	maximum mean velocity	[ms^{-1}]
u_τ	shear stress velocity	[ms^{-1}]
v	velocity component in y direction	[ms^{-1}]
w	velocity component in z direction	[ms^{-1}]
x_i	Cartesian components	[m]
x_j	Cartesian components	[m]
x_k	Cartesian components	[m]
y	Cartesian coordinate	[m]
$y+$	dimensionless wall distance	[1]
$\left(\overline{\ }\right)$	denotes mean value	
$(')$	denotes fluctuating component	

Greek symbols

α_ϕ	under relaxation factor	[1]
β_1	model coefficient (Wilcox k-ω model)	[1]
β_2	model coefficient (Menter SST k-ω model)	[1]
β^*	model coefficient (Wilcox k-ω model)	[1]
β'	model coefficient (Menter SST k-ω model)	[1]
γ_1	model coefficient (Wilcox k-ω model)	[1]
γ_2	model coefficient (Menter SST k-ω model)	[1]
Γ	diffusion coefficient	[m^{2}s^{-1}]
δ	boundary layer thickness	[m]
δ_{ij}	Kronecker delta	[1]
ε	dissipation rate	[m^{2}s^{-3}]
κ	von Karman's constant	[1]
ϑ	velocity scale	[ms^{-1}]
μ	dynamic viscosity	[kgm^{-1}s^{-1}]
μ_τ	shear stress velocity	[ms^{-1}]

μ_t	eddy viscosity	[$kgm^{-1}s^{-1}$]
ν	kinematic viscosity	[m^2s^{-1}]
ρ	density	[kgm^{-3}]
ρ'	residual	[1]
σ_k	model coefficient (k-ε model)	[1]
σ_{k-W}	model coefficient (Wilcox k-ω model)	[1]
σ_{k-SST}	model coefficient (Menter SST k-ω model)	[1]
σ_ε	model coefficient (k-ε model)	[1]
σ_ω	model coefficient (Wilcox k-ω model)	[1]
$\sigma_{\omega,1}$	model coefficient (Menter SST k-ω model)	[1]
$\sigma_{\omega,2}$	model coefficient (Menter SST k-ω model)	[1]
$\sigma_{\omega 2}$	model coefficient (Menter SST k-ω model)	[1]
τ_w	wall shear stress	[$kgm^{-1}s^{-2}$]
τ_{ij}	stress tensor	[$kgm^{-1}s^{-2}$]
ϕ	property of the fluid	
Φ	time averaged property of the fluid	
ω	turbulence frequency	[$kg^{-1}s^{-1}$]

Other symbols

∇	Laplace operator

1 Introduction

The visualization of the flow using the CFD codes is a method how to predict fluid flow without making an experiment. It can be also cheaper way of developing or improving products.

At first, in the 1930s the two-dimensional methods were developed. Later, when the sufficient computer power was available, the three-dimensional methods were introduced.

In the 1960s, a CFD techniques were developed by aerospace engineers and since then it has been improved and it is used by many others industrial areas. Moreover, it is used not only for improving human's life but also for developing medical methods for curing illnesses. The CFD was also involved in developing of the heart valve and blood pump.

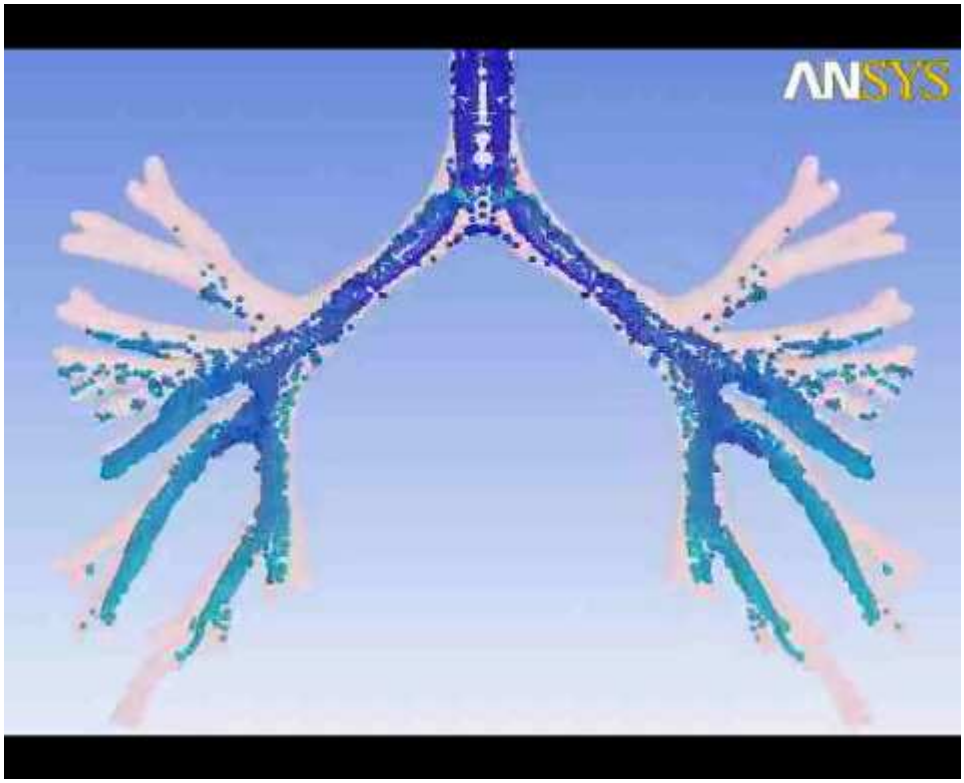

Figure 1 – Lungs breathing [8]

Nowadays it is widely used throughout industry (i.e., hydrology and oceanography, meteorology, turbo machinery, aerodynamics, electrical and electronic engineering, etc.).

At the beginning of the second part of the 20th century the engineers developed some simpler CFD codes which were intended mainly to solve some "ordinary" flow such as

combustion or model for the weather prediction but with the development of the high-performance computer there was possibility to implement more difficult models. Nowadays lots of models exist and they still have being developed.

As any others codes, a CFD code have three basic components: pre-processor, solver and post-processor.

The pre-processor allows the user to define domains, build up the physical geometry, create a mesh and tune this mesh to improve computation quality.

The solver is the main part of a CFD code. It is a collection of various algorithms and numerical techniques. CFD code is based on the discretization methods. Currently, there are three major methods. The finite element method (FEM) was developed for structural stress analysis and is not much used in fluid dynamics. Over 90 per cent of CFD codes are based on either the finite difference (FDM) or finite volume method (FVM). The latter was developed as a special formulation of the former and it is applied in most commercial CFD packages used worldwide, such as FLUET, CFX, START-CD and FLOW-3D.

The post-processor allows the user to construct a picture of the simulated flow problem, animations and graphs.

2 Mathematical Description of the Fluid Motion

2.1 General Equations of the Fluid Motion

Control Volume Equation

To study the dynamics of solid bodies it is usually used control mass (CM) as an element to be dealt with. In fluid flow it is more convenient to deal with a spatial region which is called control volume (CV).

It is considered a mass element where the fluid flows in and out of the element and the mass is neither created nor destroyed. The conservation equation can be written: [7], page 3

$$\frac{dm}{dt} = 0 \tag{2.1}$$

On the other hand, momentum can be changed by the action of forces and its conservation equation is Newton's second law of motion: [7], page 3

$$\frac{d(m\vec{u})}{dt} = \sum \vec{f} \tag{2.2}$$

If ϕ is any conserved intensive property than the integral form of the conservation equation in terms of control volume can be expressed as: [7], page 4

$$\frac{d}{dt}\int_{CM} \rho\phi dCM + \int_{S_{CV}} \rho\phi\vec{v}\cdot\vec{n}dS_{CV} = \sum \vec{f} \tag{2.3}$$

This equation is also called Reynolds´ transport theorem.

Mass Conservation

The mass conservation equation can be derived from Eq.2.3 by setting $\phi = 1$ and applying the Gauss´ divergence theorem: [2], page 13

$$\frac{\partial \rho}{\partial t} + div(\rho \vec{u}) = 0 \tag{2.4}$$

The Equation 2.4 is the unsteady, three-dimensional mass conservation or continuity equation at a point in a compressible fluid.

Momentum Equation

The momentum equation can be derived from Eq.2.3 where ϕ is replaced by *v*. Two types of forces acting on fluid particle can be distinguished. Firstly, there are surface forces such as pressure or viscous forces which are proportional to the volume of the fluid. Secondly, there are body forces such as gravity force, centrifugal force, Coriolis force and electromagnetic force which are molecular origin.

According to [7], the momentum equation is described by:

$$\frac{\partial(\rho u_i)}{\partial t} + \frac{\partial(\rho u_j u_i)}{\partial x_j} = \frac{\partial \tau_{ij}}{\partial x_j} - \frac{\partial p}{\partial x_i} + S_{Mi} \tag{2.5}$$

where τ_{ij} is a stress tensor and S_{Mi} is momentum source term.

Energy Equation

The energy equation is based on the first law of thermodynamics. The total energy of the system is the sum of the internal energy *i* and kinetic energy *k*. The internal energy *i* is a consequence of the random motion of the molecules with respect to the averaged translatory motion of the molecules and the kinetic energy *k* is due to the motion of fluid particles.

According to [2] page 18, the kinetic energy can be expressed as:

$$k = \frac{1}{2}\left(u^2 + v^2 + w^2\right) \tag{2.6}$$

where *u,v,w* are velocity components.

The total energy is [2]:

$$E = i + k \tag{2.7}$$

Then the energy equation is [2] page 19:

$$\rho \frac{DE}{Dt} = \left[-div(p\vec{u})\right] + div\left(\tau_{ij}.\vec{u}\right) + div(k'gradT) + S_E \tag{2.8}$$

The term on the left hand side is the rate of increase of energy of fluid particle. The first and second terms on the right hand side are the total rate of work done on the fluid particle by surface stresses. The third term is the rate of heat addition to the particle due to heat conduction. The last term on the right hand side is source of energy per unit volume per unit time.

General Transport Equation

The general transport equation can be derived from Eq.2.3 by specifying the sum of the forces acting on the control volume: [2], page 24

$$\frac{\partial(\rho\phi)}{\partial t} + div\left(\rho\phi\vec{u}\right) = div\left(\Gamma grad\phi\right) + S_\phi \tag{2.9}$$

Where Γ is a diffusion coefficient and ϕ is general variable and the property of the fluid. By integration Eq.2.9 and using a Gauss´s divergence theorem the Eq.2.9 becomes: [2], page 25

$$\frac{\partial}{\partial t}\left(\int_{CV}\rho\phi dV\right)+\int_{A}\vec{n}.(\rho\phi\vec{u})dA=\int_{A}\vec{n}.(\Gamma grad\phi)dA+\int_{CV}S_{\phi}dV \qquad (2.10)$$

"In time dependant problems Eq.2.10 is integrated with respect to time *t* over a small interval Δt from, say, *t* until $t+\Delta t$. This yields the most general integrated form of the transport equation:" [2], page 26

$$\int_{\Delta t}\frac{\partial}{\partial t}\left(\int_{CV}\rho\phi dV\right)dt+\int_{\Delta t}\int_{A}\vec{n}.(\rho\phi\vec{u})dAdt=\int_{\Delta t}\int_{A}\vec{n}.(\Gamma grad\phi)dAdt+\int_{\Delta t}\int_{CV}S_{\phi}dVdt \qquad (2.11)$$

If the steady state problems are solved, the first term on the left hand side in Eqs.2.10, 2.11 is zero.

2.2 Turbulent Flow

In a turbulent flow, the velocity field **u**(**x**,t) and the pressure p(**x**,t) are random, which can be characterized in terms of the mean values of flow properties ($\bar{u},\bar{v},\bar{w},\bar{p}$) and statistical properties of their fluctuations (u´,v´,w´,p´).

The Formation of the Turbulent Flow

"Essentially, small, even infinitesimal, disturbances are always present in a fluid. They may be due to small variations in properties, wall roughness, variations in free surface effects, and any other small perturbation. Under certain conditions (usually at a low Reynolds number) these disturbances damp out, and the flow remains laminar. As the Reynolds number becomes larger, infinitesimal disturbances tend to grow, and the flow is said to be unstable. Because of nonlinearities the final state of the fluid as the disturbances grow is often difficult to determine and depends critically on the configuration of the flow."[1], page 245

It can be used either mathematical description of the turbulent flow or statistical description. More difficult problems can be solved using numerical approach such as finite volume method.

The Boundary Layer

The boundary layer is a region of fluid close to the surface immersed in the flowing fluid. Figure 2 illustrates a flat face in a free fluid stream. At the surface, the velocity equals to zero ('no slip') and away from the surface rapidly increases. The zone in which this occurs is known as the boundary layer. In consequence of this, there is a velocity gradient between the fluid in the free stream and the plate surface. The shear stress τ_w is defined in this zone by: [3] page 378

$$\tau_w = \mu \frac{\partial u}{\partial y} \tag{2.12}$$

where μ is the fluid viscosity and $\frac{\partial u}{\partial y}$ is the velocity gradient.

The shear force is caused by this shear stress and the fluid close to the wall is decelerated. Further along the plate, the shear force is increased owing to the increasing surface of the plate affected by the flow and consequently the thickness of the affected fluid layer increases.

Close to the wall the flow is influenced by viscous effects and does not depend on free stream parameters. The mean flow velocity depends on the distance *y* from the wall, fluid density ρ, viscosity μ and the wall shear stress τ_w.

The law of the wall, using two dimensionless groups, u^+ and y^+ is: [2], page 57

$$u^+ = \frac{\bar{u}}{u_\tau} = f(y^+) \tag{2.13}$$

In [2] page 57 u_τ represents the shear stress velocity:

$$u_\tau = \sqrt{\frac{\tau_w}{\rho}} \tag{2.14}$$

Far away from the wall, the mean flow velocity depends on the boundary layer thickness δ, the distance *y* from the wall, fluid density ρ and the wall shear stress τ_w. Thus, according to the [2] page 58

$$\frac{\bar{u}_{\max} - \bar{u}}{u_\tau} = g\left(\frac{y}{\delta}\right) \tag{2.15}$$

This formula is called the velocity-defect law in [2].

For the meaning of the dimensionless wall velocity y^+ for the turbulence modelling see chapter 4.3.

If the turbulent flow near the wall is considered, two regions can be distinguished (Fig.2).

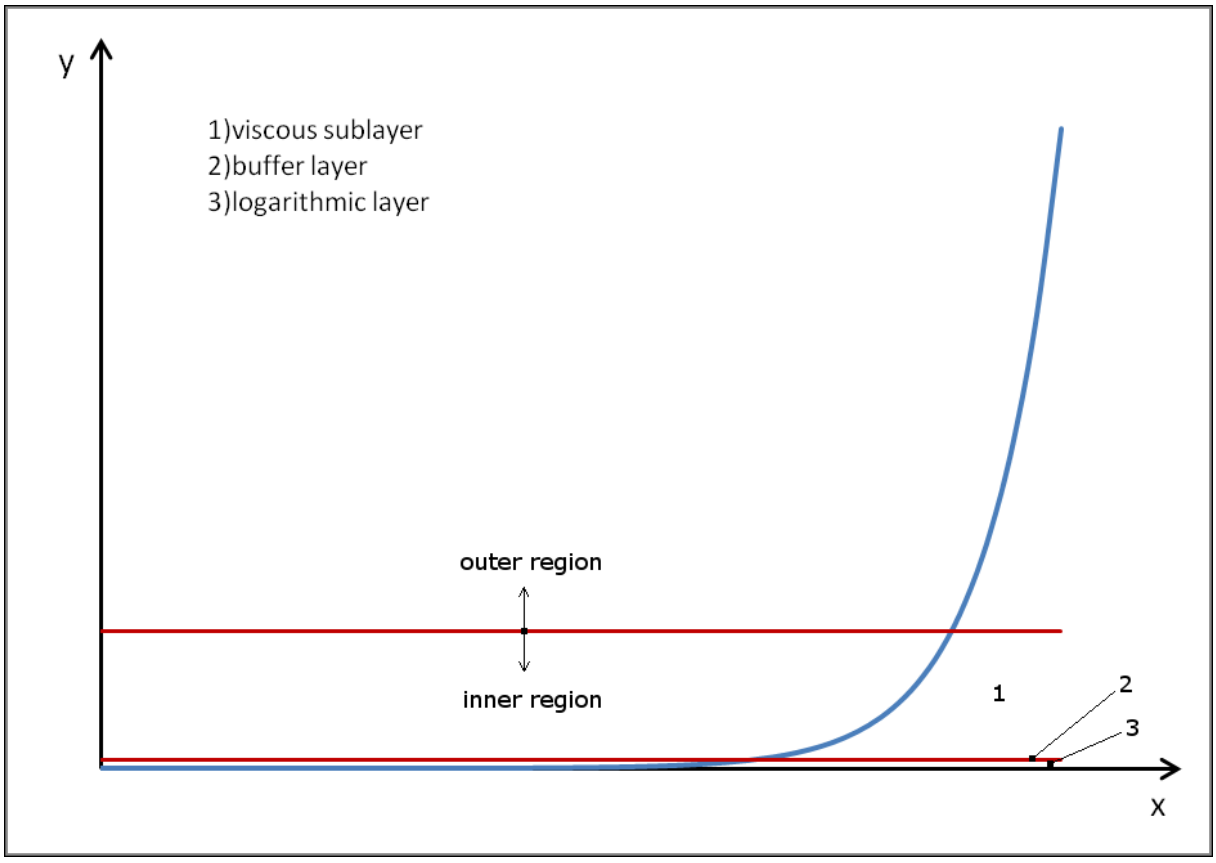

Figure 2 – The velocity history near the wall

First, inner region can be divided into tree layers:

- Viscous sublayer ($y^+ < 5$):

  The viscosity plays a dominant role in momentum and heat transfer. It may be assumed that the shear stress is approximately constant and equal to the wall shear stress τ_w.

The relationship between velocity and distance from the wall is in the viscous sublayer linear. The viscous sublayer is also called the linear sub-layer.

$$u^+ = y^+ \tag{2.16}$$

- Buffer layer

  The viscous stresses and turbulent stresses are of similar magnitude.

- Logarithmic layer ($50 < y^+ < 500$) [2]

In this layer, turbulent stresses dominate. The shear stress τ varies slowly with the distance from the wall. The logarithmic profile approximates the velocity distribution. Moreover, the relationship between velocity and the distance from the wall is also logarithmic: [2], page 58

$$u^+ = \frac{1}{\kappa}\ln\left(y^+\right) + B = \frac{1}{\kappa}\ln\left(E * y^+\right) \tag{2.17}$$

This formula is called log-law and this layer is called log-law layer as well. In Eq.2.17, the constant κ is von Karman's constant ($\kappa = 0.4$) and B and E^* are additive constants ($B = 5.5$ and $E^* = 9.8$). The values of constants B and E^* are intended for the smooth walls. With the increasing roughness of the wall, the constants B and E^* decreases. Thus the dimensionless wall distance is calculated according to [2] with formula:

$$y^+ = \sqrt{y} \cdot \sqrt{\frac{\overline{u}_{FS}\rho}{\mu}} \tag{2.18}$$

where y is a first prism height and $\overline{u}$ is the free stream velocity.

In the second, the outer region, the viscous effects can be neglected. In this region, inertia forces dominated and the velocity is not changed a lot and equals to the free stream velocity.

2.3 Equations of Motion for Turbulent Flow

Continuity Equation

Derived equation 2.4 is also valid for turbulent flow. If there is taken the time average of this equation using Reynolds rules of averages, there is obtained: [1], page 248

$$\frac{\partial \overline{\rho}}{\partial t} + \frac{\partial}{\partial x_i}\left(\overline{\rho}\,\overline{u_i}\right) + \frac{\partial}{\partial x_i}\overline{\left(\rho' u_i'\right)} = 0 \tag{2.19}$$

For incompressible flow, equation 2.19 becomes

$$\frac{\partial \overline{u_i}}{\partial x_i} = 0 \tag{2.20}$$

Reynolds Equation

Using the averaged notation and Eq.2.5, the averaged Navier-Stokes equation in vector form is given by: [1]

$$\frac{\partial\left(\overline{u}\right)}{\partial t} + div\left(\overline{u}\,\overline{u}\right) = -grad\left(\frac{\overline{p}}{\rho}\right) + \mu\nabla^2\overline{u} - div\left(\overline{u'u'}\right) \tag{2.21}$$

Transport Equation

As well as the commonalities among continuity, momentum and energy equations are, in general equations for fluid motion, there are the same commonalities among these equations in turbulent flow. The time averaged transport equation for scalar ϕ is: [2], page 64

$$\frac{\partial \Phi}{\partial t} + div\left(\Phi\overline{u}\right) = \frac{1}{\rho} div\left(\Gamma_\Phi grad\Phi\right) + \left[-\frac{\partial \overline{u'\varphi'}}{\partial x} - \frac{\partial \overline{v'\varphi'}}{\partial y} - \frac{\partial \overline{w'\varphi'}}{\partial x}\right] + S_\Phi \tag{2.22}$$

3 Turbulence Models

The turbulence models are used to describe turbulent flow in more or less sufficient way with using computers. Many of them are widely used in the general-purpose CFD. Nowadays there exist lots of turbulence models. They are used more or less to describe flows which are usually present in the ordinary life. Other was developed to solve more difficult problems such as the space shuttle going from space to the earth atmosphere. For this problem models such as the Direct Simulation Monte Carlo (DSMC) are used.

Among classical turbulence models can be included the mixing length model, k-ε model, k-ω model, RSM model, RNG model, Spalart-Allmaras model or ASM model for anisotrophy fluids.

3.1 Classical Turbulence Models

There are many models which can be used in the description of the turbulent flow. These models are usually used in the computational approach to solve the Eqs 2.4, 2.5 using discretization by means of finite difference method or finite volume method. Moreover the equations which describe turbulent motion are solved.

Some of the classical turbulence models such as the mixing length and k-ε model are based on the presumption that there exists an analogy between the action of the viscous stresses and Reynolds stresses on the mean flow. Both stresses appear in the momentum equation.

Reynolds stresses might be proportional to mean rates of deformation. So the Reynolds stresses are described by the Boussinesq relationship: [2], page 67

$$\tau_{ij} = -\rho\overline{u_i' u_j'} = \mu_t\left(\frac{\partial \overline{u}_i}{\partial x_j} + \frac{\partial \overline{u}_j}{\partial x_i}\right) - \frac{2}{3}\rho k \delta_{ij} \tag{3.1}$$

μ_t is eddy viscosity and δ_{ij} is the Kronecker delta ($\delta_{ij} = 1$ if i=j and $\delta_{ij} = 0$ if $i \neq j$) and *k* is the turbulent kinetic energy.

Mixing Length Model

The mixing length model is an algebraic zero equation model and can be applied to free shear flows. This model is based on the Reynolds stresses and viscous stresses on the mean flow.

The advantage of this model is that it is easy to implement it. Nevertheless, many of the fluid flow cannot be described by such simple formulae, so the mixing length model is used in the CFD software only for rough prediction of the fluids behaviour.

The k-ε Model

The k-ε model belongs to the class of two-equation models, in which model transport equations are solved for two turbulence quantities – i.e., k and ε in the k-ε model.

The k-ε model is the most widely used complete turbulence model which is incorporated in most commercial CFD codes. It can be used to describe problems where the mixing length model is insufficient, i.e., if convection and diffusion are not negligible, the mixing length model is no longer feasible.

The k-ε model consist of

1/ the model transport equation for k (governing equation for turbulent kinetic energy)

2/ the model transport equation for ε (governing equation for dissipation rate)

Firstly, some preliminary definitions are mentioned.

The velocity scale ϑ and length scale l are as follows according to [2] page 75

$$\vartheta = k^{1/2} \qquad l = \frac{k^{3/2}}{\varepsilon} \tag{3.2)(3.3}$$

The definition of the eddy viscosity for using in k-ε model is as follows according to [2] page 75

$$\mu_t = \rho C_\mu \frac{k^2}{\varepsilon} \tag{3.4}$$

Where C_μ is a dimensionless constant.

The standard k- ε model is described by: [2] page 75

$$\frac{D(\rho k)}{Dt} + div(\rho k\bar{u}) = div\left(\frac{\mu_t}{\sigma_k} grad(k)\right) + 2\mu_t S_{ij} \cdot S_{ij} - \rho\varepsilon \tag{3.5}$$

$$\frac{D(\rho \varepsilon)}{Dt} + div(\rho \varepsilon\bar{u}) = div\left(\frac{\mu_t}{\sigma_\varepsilon} grad\varepsilon\right) + C_{1\varepsilon}\frac{\varepsilon}{k} 2\mu_t S_{ij} \cdot S_{ij} - C_{2\varepsilon}\rho\frac{\varepsilon^2}{k} \tag{3.6}$$

The model constants are: [2] page 75

$$C_\mu = 0.09\,;\sigma_\varepsilon = 1.30\,;\sigma_k = 1.00\,;C_{1\varepsilon} = 1.44\,;C_{2\varepsilon} = 1.92 \tag{3.7 a-e}$$

Using Boussinesq relationship, the Reynolds stresses are computed by formula 3.1.

Reynolds Stress Equation Models

The Reynolds stress equation model is seven equations model and belongs to the group which is the most complex classical turbulence model. It attempts to predict flows with complex strain fields or significant body forces. In this model, transport equations are solved for six independent Reynolds stresses

$$-\rho\overline{u_1'^2}\,;\,-\rho\overline{u_2'^2}\,;\,-\rho\overline{u_3'^2}\,;\,-\rho\overline{u_1'u_2'}\,;\,-\rho\overline{u_1'u_3'}\,;\,-\rho\overline{u_2'u_3'} \tag{3.8 a-f}$$

Therefore, the six transport equations for Reynolds stresses and an equation for the scalar dissipation rate ε can be solved but because of the high cost of the computations it is not so widely used in industrial flow.

3.2 Advanced Turbulence Models

There are some models which can be included in the advanced turbulence models such as two layer k-ε model which uses different treatment of the fully turbulent region and viscous region.

Another model, the RNG k-ε model is based on renormalization group analysis of the Navier-Stokes equations. It removes the small scales of motion from the governing equation by expressing their effects in terms of large scale motions and modified viscosity.

There is also another model which deals with zero pressure gradient and adverse pressure gradient boundary layer better than previous models. The most suitable for general purpose CFD are Wilcox k-ω model and SST k-ω model. Spalart-Allmaras model can be also included in this category but it lacks sensitivity to transport processes in rapidly changing flows.

Wilcox k-ω Model

The Wilcox k-ω model is two equations model based on the k-ε model. This model uses the turbulence frequency ω as the second variable: [2]

$$\omega = \frac{\varepsilon}{k} \tag{3.9}$$

Therefore, the eddy viscosity is given by [2]

$$\mu_t = \rho \frac{k}{\omega} \tag{3.10}$$

The equation 3.1 is valid to obtain Reynolds stresses.

The transport equation for k and ω for turbulent flows at high Reynolds number is as follows: [2] page 90

$$\frac{\partial(\rho k)}{\partial t} + div(\rho k\bar{u}) = div\left[\left(\mu + \frac{\mu_t}{\sigma_k}\right) grad(k)\right] + P_{ij} - \beta^* \rho k \omega \tag{3.11}$$

The second term on the right hand side is the rate of production of turbulent kinetic energy: [2] page 90

$$P_{ij} = \left(2\mu_t S_{ij} \cdot S_{ij} - \frac{2}{3}\rho k \frac{\partial \bar{u}_i}{\partial x_j}\delta_{ij}\right) \tag{3.12}$$

The ω transport equation is: [2] page 90

$$\frac{\partial(\rho\omega)}{\partial t} + div(\rho\omega\bar{u}) = div\left[\left(\mu + \frac{\mu_t}{\sigma_\omega}\right) grad(\omega)\right] + \gamma_1\left(2\rho S_{ij} \cdot S_{ij} - \frac{2}{3}\rho\omega\frac{\partial \bar{u}_i}{\partial x_j}\delta_{ij}\right) - \beta_1 \rho\omega_2 \tag{3.13}$$

The constants included in Eqs 3.10, 3.12 are: [2] page 90

$$\sigma_{k-w} = 2.0\,;\sigma_\omega = 2.0\,;\gamma_1 = 0.553\,;\beta_1 = 0.075\,;\beta^* = 0.09 \tag{3.14 a-e}$$

This model is suitable for general-purpose CFD.

Menter SST k-ω Model

The Menter SST k-ω model is based on the k-ε model. Because of the less sensitivity of the k-ε model in the free stream and its unsatisfactory near-wall performance, SST k-ω model was developed. It uses a transformation of the k-ε model into k-ω model in the near-wall region and the standard k-ε model in the fully turbulent region. Since this transition can cause numerical instabilities the blending functions are used to achieve a smooth transition. "The blending functions are critical to the success of the method. Their formulation is based on the distance to the nearest surface and on the flow variables." [9]

The blending functions F_1 and F_2 are formulated as: [9]

$$F_1 = \tanh\left(\min\left(\max\left(\frac{\sqrt{k}}{\beta'\omega y}, \frac{500\nu}{y^2\omega} \right), \frac{4\rho k}{CD_{k\omega}\sigma_{\omega 2} y^2} \right) \right)^4 \tag{3.15}$$

$$F_2 = \tanh\left(\max\left(\frac{2\sqrt{k}}{\beta'\omega y}, \frac{500\nu}{y^2\omega} \right) \right)^2 \tag{3.16}$$

where model constants are: [9]

$$\sigma_{\omega 2} = 1/0.856 ; \beta' = 0.09 \tag{3.17}$$

and according to [9]

$$CD_{k\omega} = \max\left(2\rho \frac{1}{\sigma_{\omega 2}\omega} \nabla k \nabla \omega, 1.0\times 10^{-10} \right) \tag{3.18}$$

With using substitution $\varepsilon = k\omega$ the SST k-ω model transport equation is described by: [2] page 91

$$\begin{aligned} &\frac{\partial(\rho\omega)}{\partial t} + div(\rho\omega\bar{u}) = \\ &= div\left[\left(\mu + \frac{\mu_t}{\sigma_{\omega,1}} \right) grad(\omega) \right] + \gamma_2 \left(2\rho S_{ij} \cdot S_{ij} - \frac{2}{3}\rho\omega \frac{\partial U_i}{\partial x_j}\delta_{ij} \right) - \beta_2 \rho\omega_2 + 2\frac{\rho}{\sigma_{\omega,2}\omega} \frac{\partial k}{\partial x_k} \frac{\partial \omega}{\partial x_k} \end{aligned} \tag{3.19}$$

Last term on the right hand side is the cross-diffusion term, which arises during the transformation.

The model constants are: [2] page 91

$$\sigma_{k-SST} = 1.0 ; \sigma_{\omega,1} = 2.0 ; \sigma_{\omega,2} = 1.17 ; \gamma_2 = 0.44 ; \beta_2 = 0.083 ; \beta' = 0.09 \qquad \text{(3.20 a-f)}$$

The last equation which is solved by the SST model is wall scale function. Using wall functions are the most popular way to account for wall effects. The example of the wall function is Eqs 2.17 or 2.19 but there exist also most generalized functions using for the

description of the viscosity near the wall the piecewise linear functions. The more detailed description of the wall functions can be found in [11].

This model provides good near-wall behaviour of the fluid flow. On the other hand, it has some limiters which prevent the build-up of turbulence in stagnation regions. The SST model is recommended by [9] for high accuracy boundary layer simulation.

4 CFD Analysis

The CFD analysis of the fluid flowing around the fuselage of the aircraft is made in CFX software using Ansys 12.0 Workbench interface. The properties of the hardware configuration are stated in Table 1.

Notebook HP Pavilion dv6-2160ec	
RAM	DDR 3 4GB
processor	Intel Core i5-520M, 2.4GHz
grafická karta	NVIDIA GeForce GT320M 1 GB

Table 1 – The hardware configuration

The CFD analysis is divided into the three parts. At first, pre-processor with the modelling part and meshing part is stated then solution process is described and finally the results are discussed.

4.1 Pre-processor

Model Description

The CFD analysis is performed on a modern, twin-engine, model of the transport aircraft with transonic wing-body design denoted DLR-F6 which is depicted with the main dimensions in Figure 3. The missing dimension in Figure 3 is the mean aerodynamic chord which is 5.559inches or 0.14m. This aircraft is similar to Boeing 737 (types without winglets) or Boeing 767-400 depicted in Figure 4. The DLR-F6 is designed for a cruise of Mach number M=0.75 and a designed lift coefficient of C_L=0.5. It is a standard model used for the tests in wind tunnel. On account of the using of the DLR-F6 in wind tunnel, there are no tail wings which can be seen in Figure 5 which represents the CAD model of the DLR-F6.

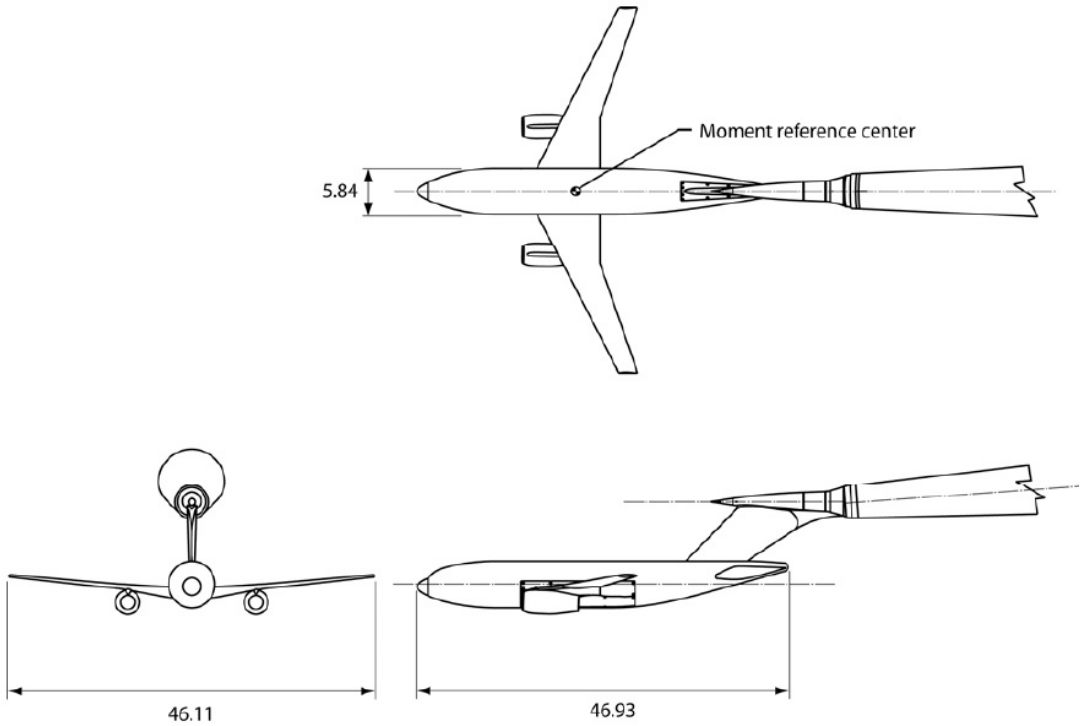

Figure 3 – The main dimensions of the DLR-F6 (distances in inches) [10]

Figure 4 – Boeing 767-400 [5]

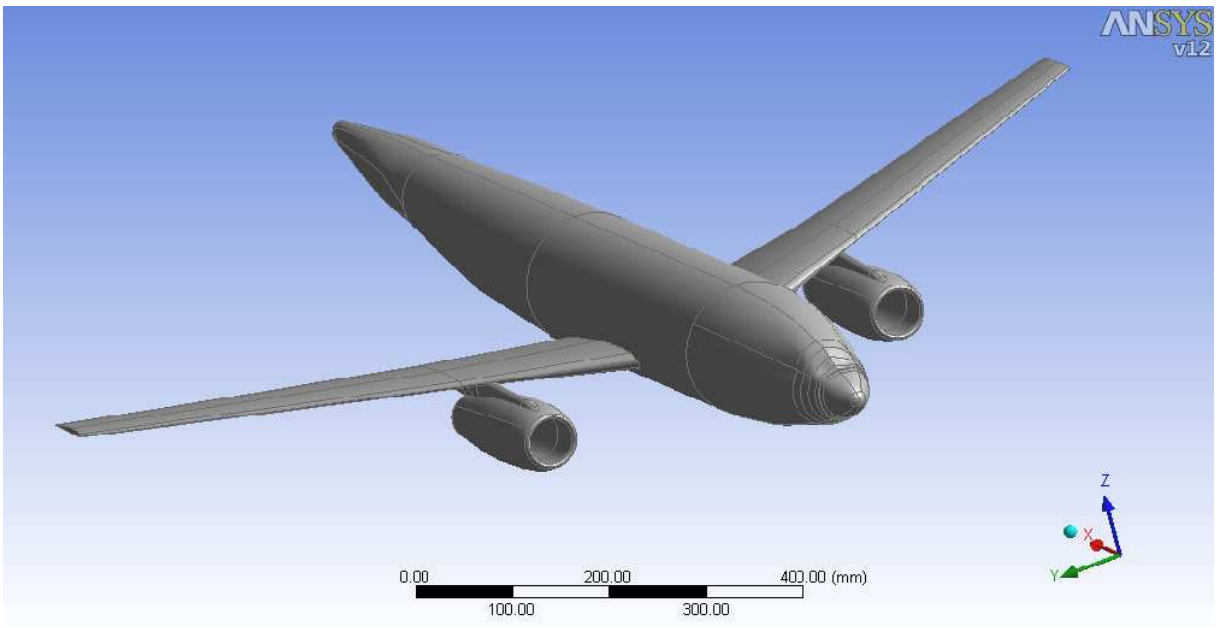

Figure 5 – The CAD model of the DLR-F6 aircraft

CAD Model Adaptation to CFD Analysis

The simplifications are usually used to reduce the number of elements and speed up meshing and solution process. The most frequent simplification is the use of the symmetry planes where it is possible. Since the DLR-F6 model is symmetric along its vertical middle plane so the model will be analyzed in symmetry in order to reduce the number of mesh elements and consequently reduce the solution time and cost.

The features of the model or domain which are not necessary for the solution should be also removed. It can be the screw holes or in the case of the aircraft, the Pitot tube. These parts can cause the mesh refinement which is unfavourable and unnecessary. Then the model is prepared for the calculation.

It is also necessary to create a fluid domain around the solid object of the aircraft by "printing" (Boolean's operation subtract the half CAD model of the aircraft from the block with the given dimensions) it into the block whose features are shown in Figure 6. The depth of the block is 1 171mm. This model of the aircraft is now prepared for the mesh generation.

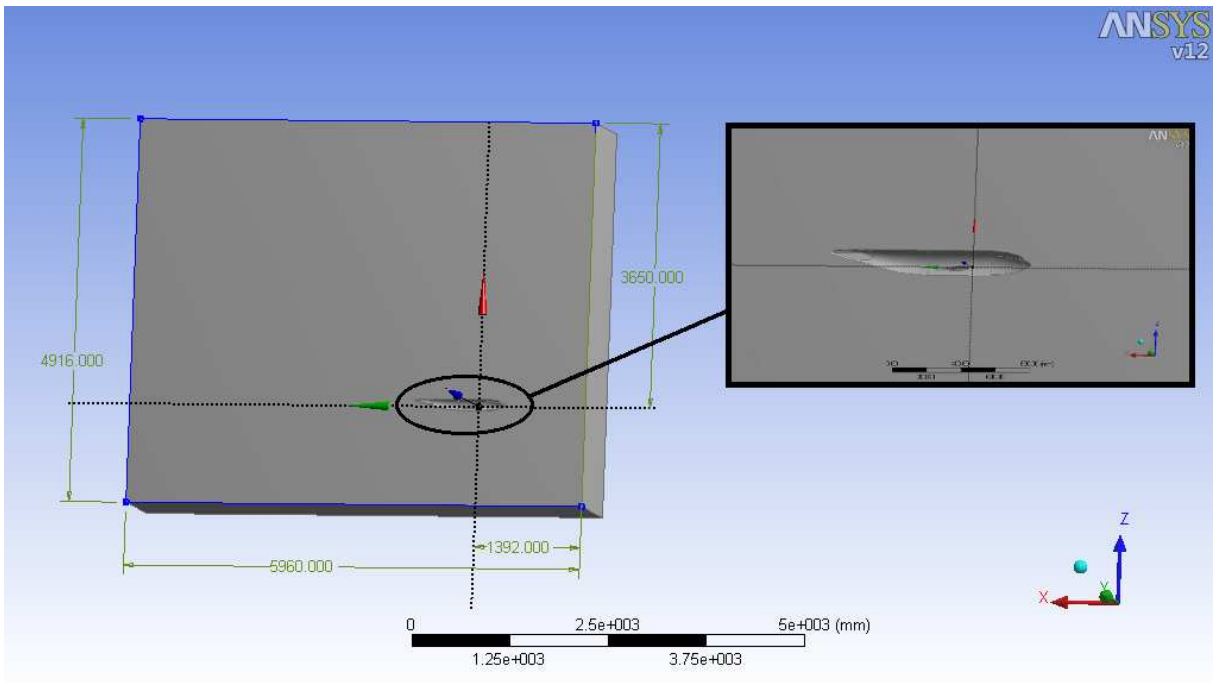

Figure 6 – The dimensions of the fluid domain

4.1.1 Mesh Generation

The mesh density and the scatter of the mesh elements should be adequate to the analysis which will be performed. The size of the 3D elements should be adequate mainly to the location of the element. Thus the element should be greater close to the surface of the aircraft and its size can be enlarged in the direction outside the surface of the aircraft. Also the shapes of the elements are different. In the boundary layer there is more comfortable to use prisms elements whereas in the bulk can be use other types of elements such as pyramids and tetrahedral elements.

The mesh of the faces consists of the triangular elements or rectangular elements and consequently the mesh of the domain consists of the tetrahedral or pyramidical elements and prism or wedge elements which usually creates boundary layer. These elements are depicted in Figure 7.

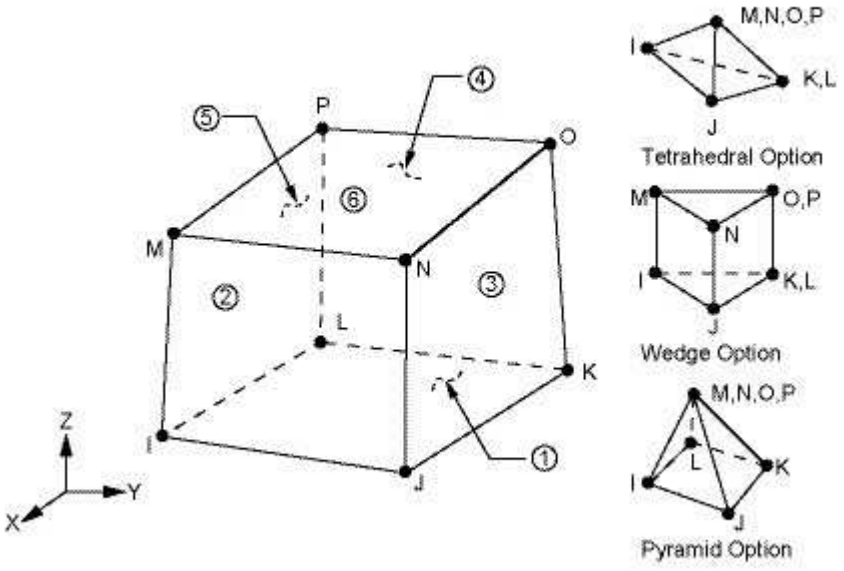

Figure 7 – The elements used in the CFD analysis

The Boundary Layer

It is necessary to create a boundary layer around the aircraft in order to distinguish the velocity change near the wall of the aircraft.

The boundary layer around the aircraft was created by the 10 inflation layers with the first prism height 1.4mm and expansion factor 1.3. The expansion factor is according to [9] a number in the range from 1.0 to 1.5 which specifies how fast the mesh length scale returns to its background value away from a region where it has been constrained. Since the value of the first prism height is the only variable which can be changed in the formula (Eq.2.18) it plays one of the most important roles in the near wall visualization of the flow. The boundary layer in the symmetry plane is shown in Figure 8.

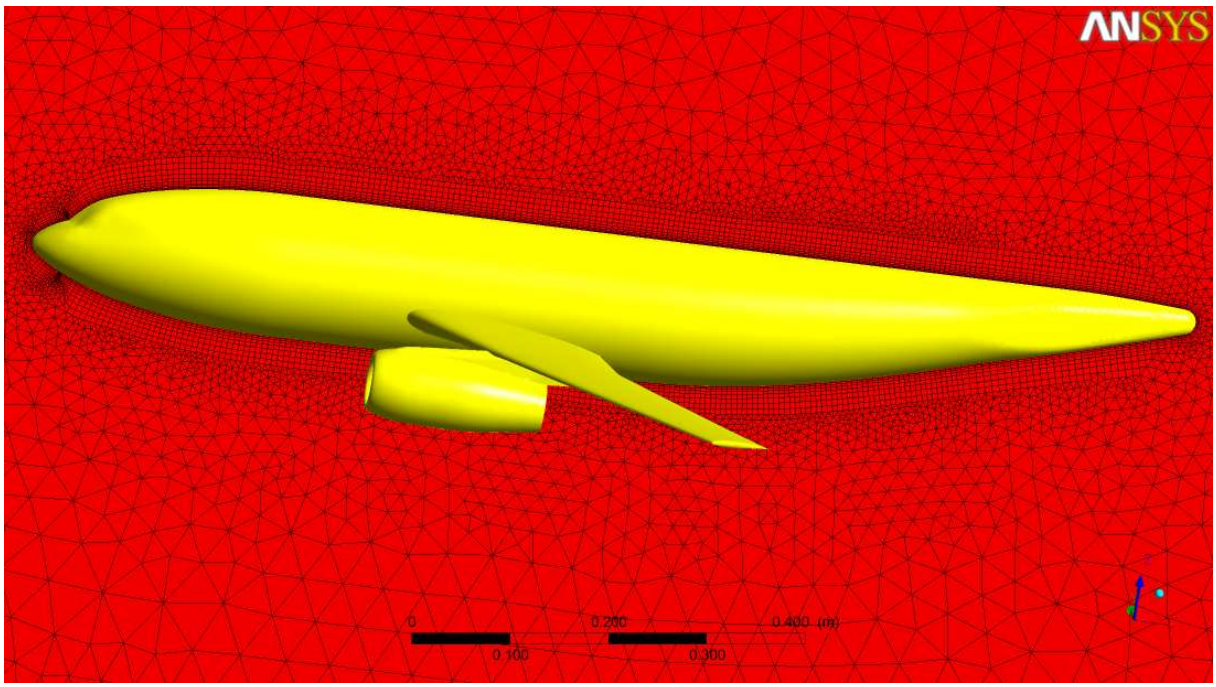

Figure 8 – The mesh around the fuselage in the symmetry plane

Mesh of the Faces

One of the biggest limitations for creating mesh in the fluid domains was the hardware configuration. The maximum number of the elements which could be solved was approx. 9 millions.

The aim of this part was the best resolution of the wing faces where the major component of the lift and drag force is present. On that account the mesh elements are finer on the wing and coarser on the fuselage surfaces (Fig. 9). In the vicinity of the wing there was not possible to achieve sufficient resolution to provide better results. The mesh in the vicinity of the wing is depicted in Figure 10. The detail view in Figure 10 shows that the transition between fin elements and coarse elements is very quick and errors can appear.

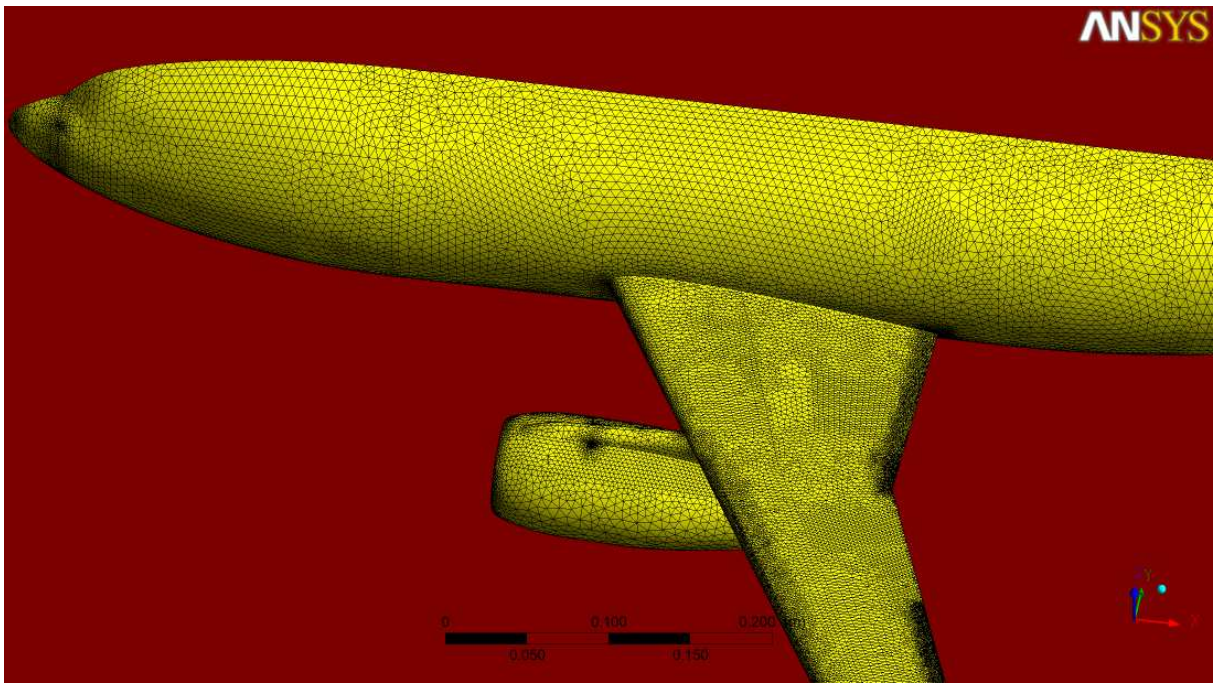

Figure 9 – The surface mesh of the aircraft

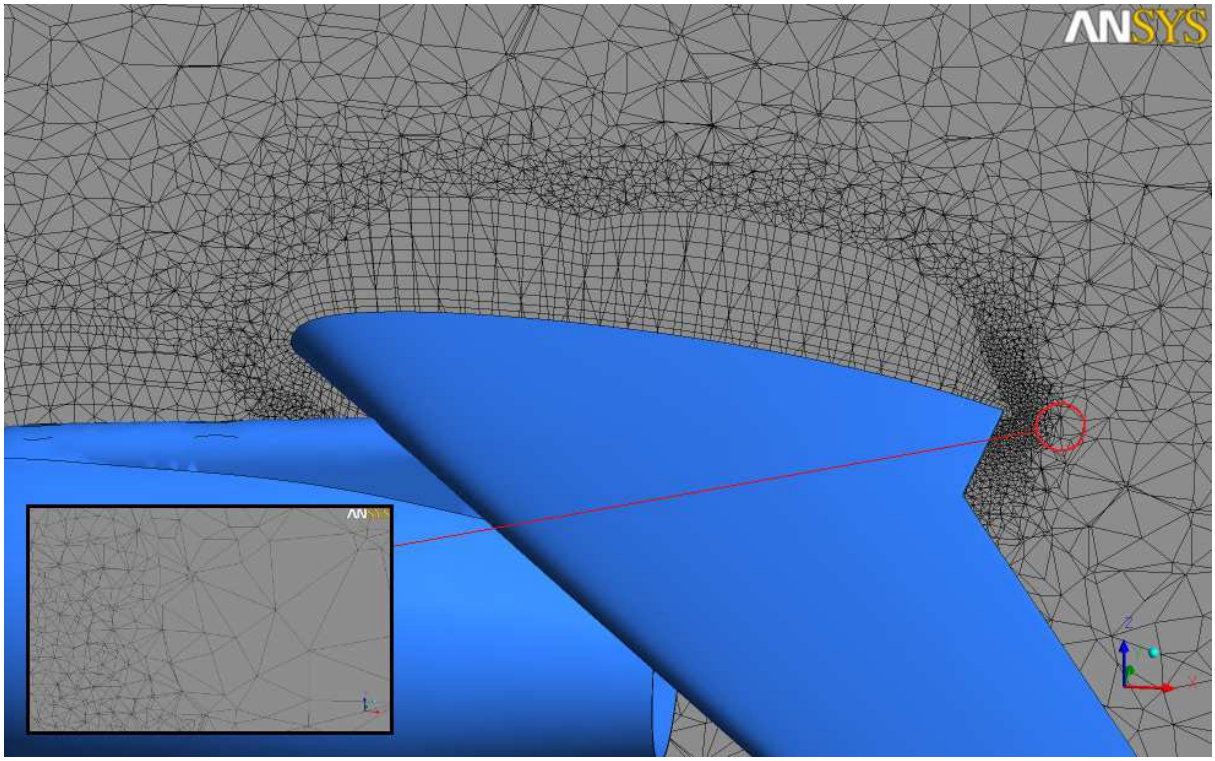

Figure 10 – The mesh in the surrounding of the wing

The Specification of the Free Stream

The aircraft was considered in the cruise in the 8 kilometres above the sea level. The main features of the air in this altitude are stated in Table 2. The changes in the air features during descending or climbing were not considered because the change of the properties is not so big to influence results significantly and the main affection of the results will be caused by the unsatisfactory size of the elements.

Property	*Symbol*	*Value*	*Dimension*
density	ρ	0.52578	kgm^{-3}
pressure	p	35 651	$kgm^{-1}s^{-2}$
speed of the sound	a_∞	308.11	ms^{-1}
temperature	T	236.215	K
dynamic viscosity	μ	$1.5271.10^{-5}$	$kgm^{-1}s^{-1}$

Table 2 – The air features at 8km above the sea level [4]

The Features of the Flow

It is considered the flow of the real viscous fluid which can be turbulent. The turbulent flow means that the particles of the fluid have two velocity components of the velocity vector namely mean velocity and fluctuating velocity. The velocity vector has tree components – x, y, z – so the flow is 3D. Since the velocity does not depend on time, the flow is steady. It is considered the stationary aircraft in the flow of the air. It means that in reality the aircraft flies through stationary air.

The Characteristic Numbers

First number which characterizes the flow around the aircraft is Reynolds number. According to the [4], page 68 Reynolds number is calculated with formula:

$$\mathrm{Re} = \frac{\rho \bar{u}_{FS} L}{\mu} \tag{4.1}$$

where $\overline{u}_{FS}$ is free stream velocity and L is the characteristic length (e.g., the chord of the wing).

Second number which characterizes the flow is Mach number. According to the [4], page 68 Mach number is calculated with formula:

$$Ma = \frac{\overline{u}_{FS}}{a_{\infty}} \tag{4.2}$$

where a_{∞} is the speed of sound in the medium.

For the calculation of the aircraft the aforementioned numbers has the value:

1. Reynolds number

$$\mathrm{Re} = \frac{0.52578 \cdot \frac{850}{3.6} \cdot 0.14}{1.5271.10^{-5}} = 1.14.10^{6}[1] \tag{4.3}$$

2. Mach number

$$Ma = \frac{\frac{850}{3.6}}{308.11} = 0.77[1] \tag{4.4}$$

4.1.2 Boundary Conditions

Five most common boundary conditions namely inlet, outlet, symmetry, wall and opening can be implemented.

The value of the velocity is usually specified at the inlet but also other values such as pressure can be specified. However these specifications are not very common. The specific values for the turbulent flow such as turbulent kinetic energy and turbulent dissipation rate

can be also specified. The inlet boundary condition is used where the flow is predominantly directed into the domain.

On the other hand the outlet boundary condition is used where the flow is predominantly directed out of the domain. The boundary condition specification for a subsonic outlet involves some constraint on the boundary static pressure, velocity or mass flow. For all other transport equations, the outlet value of the variable is part of the solution. [8] Also for the outlet the specification of the turbulent kinetic energy and turbulent dissipation rate can be used.

The symmetry boundary condition is used where the mirror plane is defined.

The opening boundary condition allows the fluid to cross the boundary surface in either direction. Again same values such as velocity or pressure etc. can be specified and for turbulent flow turbulent kinetic energy and turbulent dissipation rate can be used.

The walls are solid and impermeable boundaries. Some features can be specified such as roughness, mass and momentum of the wall or its velocity (e.g., for the blade of the turbine - rotating wall).

Boundary Conditions Applied to the Model

The velocity was set in the x-direction to the value of 850kmh^{-1} for the cruise. For the climb and descend the velocity was set by components of the velocity vector according to the angle of attack of 10 degrees. This angle was chosen as the angle where there is possible to observe phenomena occurring around the wing which does not cause the unexpected behaviour (e.g., the crash of the aircraft). There is also turbulence specification at the inlet. The intensity of the turbulence going into domain is set to 1%. The same value was used for opening and outlet. The location of the inlet is depicted in Figure 11 by yellow colour.

The outlet was specified through zero relative static pressure. The location of the outlet is depicted in Figure 11 by green colour.

The symmetry does not require any specification. The location of the symmetry is depicted in Figure 11 by red colour.

The wall is specified by the roughness, mass and momentum condition. The wall is smooth with no slip velocity. It means that the velocity immediately next to the wall is zero. The location of the wall is depicted in Figure 11 by blue colour.

The opening boundary condition was also specified by zero relative static pressure. The opening boundary condition is applied to the rest of the sides of the block which are not denoted in Figure 11.

Since the aforementioned feature of the outlet says that the flow was predominantly directed out of the domain, the boundary condition for climb and descent must be changed. So at the outlet there is an opening boundary condition to not allow fluid to be taken in the domain.

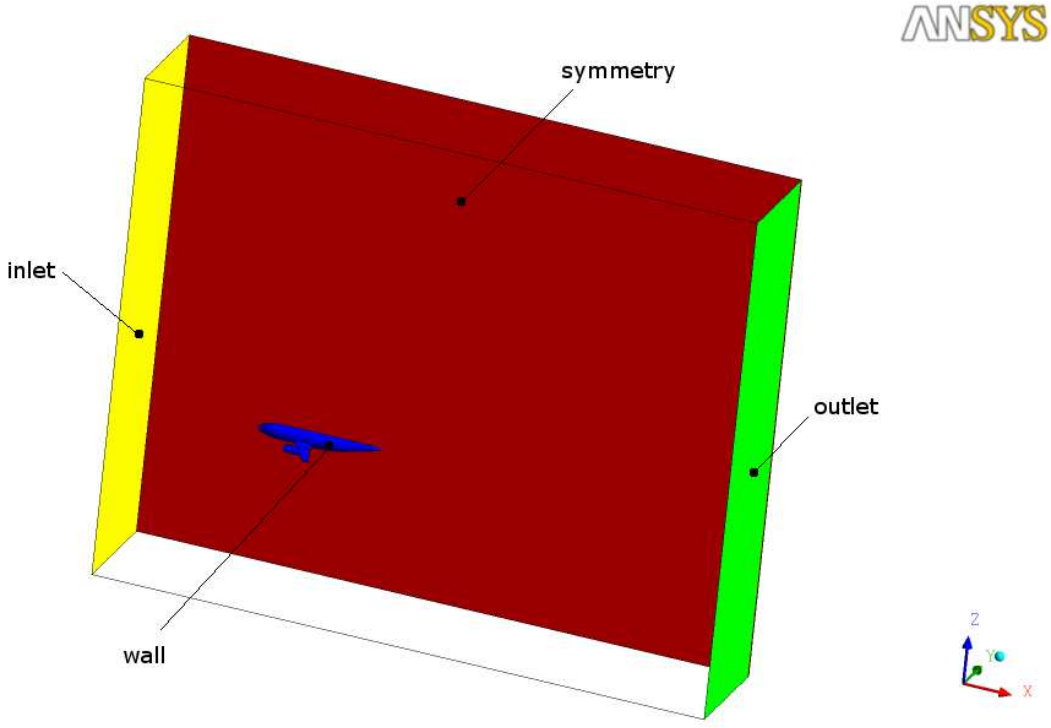

Figure 11 – The location of the boundary planes

The value of the turbulent kinetic energy and turbulent dissipation rate can be also set into the boundary conditions. Its value is as follows:

1. Turbulent kinetic energy *k* according to [2], page 77

$$k = \frac{2}{3}(\bar{u}T_i)^2 = \frac{2}{3}\left(\frac{850}{3.6}\cdot 0.01\right)^2 = 3.72\left[m^2 s^{-2}\right] \tag{4.5}$$

where $\bar{u}$ is free stream velocity and T_i represents turbulent intensity which was set to 1%.

2. Turbulent dissipation rate ε according to [2], page 77

$$\varepsilon = C_\mu^{3/4}\frac{k^{3/2}}{0.07L^*} = 0.09^{3/4}\frac{3.72^{3/2}}{0.07\cdot 4.916} = 3.43\left[m^2 s^{-3}\right] \tag{4.6}$$

where L^* is the main dimension at the inlet.

4.2 Solution

Solver Options Setting

The fluid flowing through the domain was solved as steady state. Since the flow is turbulent two models can be chosen for solving the flow around the fuselage of the aircraft. First model, k-ε model, is usually used to solve problems in engineering field. On the other hand, the Menter SST model is recommended for external aerodynamics solution and for its good resolution of the near wall flow and adverse pressure gradient.

Also the differencing scheme for either set of equations can be chosen. The differencing scheme is a way of obtaining the discritezed equation by means of FVM or FDM. For a momentum and mass equations the higher order scheme was chosen whereas for the turbulence equations the first order scheme was chosen. It is because the higher order schemes give in this case very unstable results.

The Convergence Judging - The Theoretical Background

The exact solution of the general transport equations is possible to solve analytically only for some simple examples or for that problems where approximation could be realized. However if the approximation is done, the errors appear. According to [7], in most cases, the numerical methods have to be used. Firstly, the equations must be discretized using finite difference of finite volume method where errors appear during the solution process. Then, they are solved using direct or iterative methods. These methods are based on Gauss elimination or LU decomposition according to [7].

The errors are unavoidable in the numerical solution of the fluid flow problems. They appear from the beginning of the solution process to its end. The difference between exact solution of the conservative equations and approximate solution is a non-zero residual. The purpose of the iteration procedure is to drive the residual to zero.

At the beginning the matrix equation is solved: [7]

$$[A]\{\phi\} = [Q] \tag{4.7}$$

Where A is a matrix of the coefficients, ϕ is a vector of an unknown property and Q is a vector of source terms.

This equation is iterated and after *n*th iterations the equation is of form: [7]

$$A\phi^n = Q - \rho'^n \tag{4.8}$$

Where ρ' is a non-zero residual.

The solution of the equation is finished when the required accuracy was reached.

Under Relaxation Factors

The under relaxation factors are used to obtain better convergence and damp down the bouncing convergence behaviour. On the *n*th outer iteration the algebraic equation for a variable ϕ may be written: [7]

$$A_P \phi_P^n + \sum_l A_l \phi_l^n = Q_P \tag{4.9}$$

where subscript *l* represents all faces of the element. ϕ^{n-1} may be involved in the coefficients A_l and the source Q. The Eq.4.9 could cause instability so at the beginning of the iteration process we allow ϕ^n to change only a fraction α_ϕ of the would-be difference and with increasing number of iterations the value of α_ϕ is also increased and tends to unity. In [7] is used a modification of the Eq.4.9 in form:

$$\frac{A_P}{\alpha_\phi} \phi_P^n + \sum_l A_l \phi_l^n = Q_P + \frac{1-\alpha_\phi}{\alpha_\phi} A_P \phi_P^{n-1} \tag{4.10}$$

In CFD codes the under relaxation factor has a form:

$$under\_relaxation\_factor = \frac{1}{\alpha_\phi} \tag{4.11}$$

So at the beginning the value of the under relaxation factor is used close to the unity and is stepwise decreased. The value of the under relaxation factors are usually in range:

$$0 \le \alpha_\phi \le 1 \tag{4.12}$$

The Convergence Judging

The accuracy was set to 1E-5 which is good convergence sufficient for most engineering applications and recommended by [9]. Since the problem with convergence has arisen from the solution with k-ε model it was solved with Menter SST model. In Figure 12 and 13 there

are depicted the difference between the convergences which was obtained by k-ε model and SST model. In Figure 12 there is a residuals history obtained by k-ε model where the required accuracy was not reached after 50 iterations. On the other hand, in Figure 13 the convergence was reached after 42 iterations using SST model.

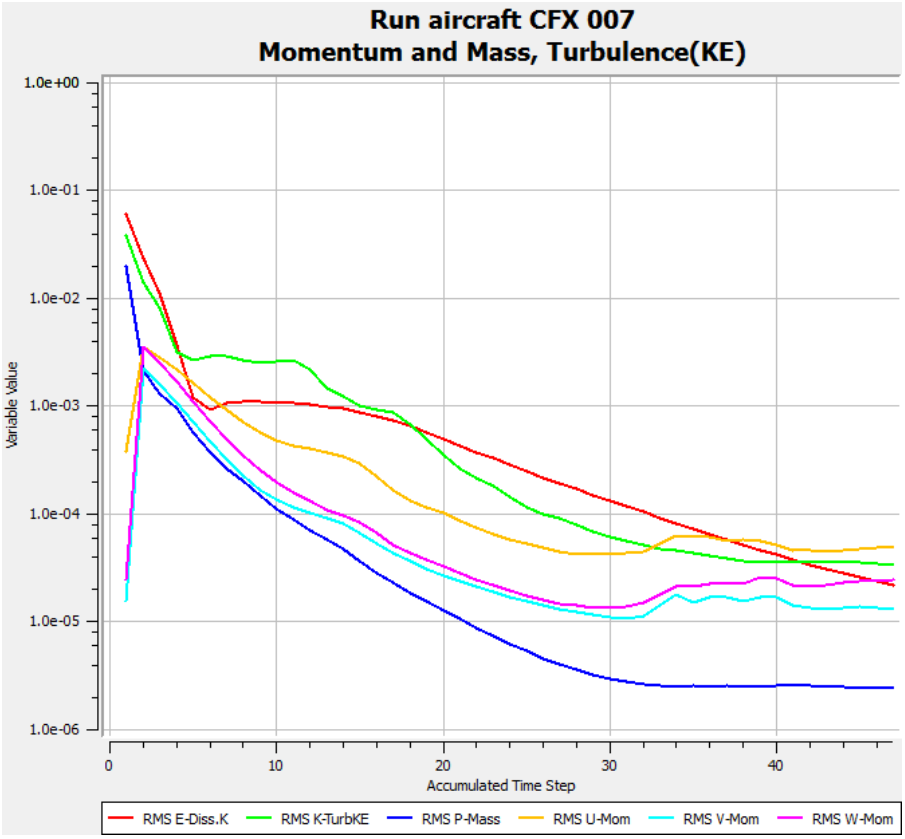

Figure 12 – The residuals history (k-ε model)

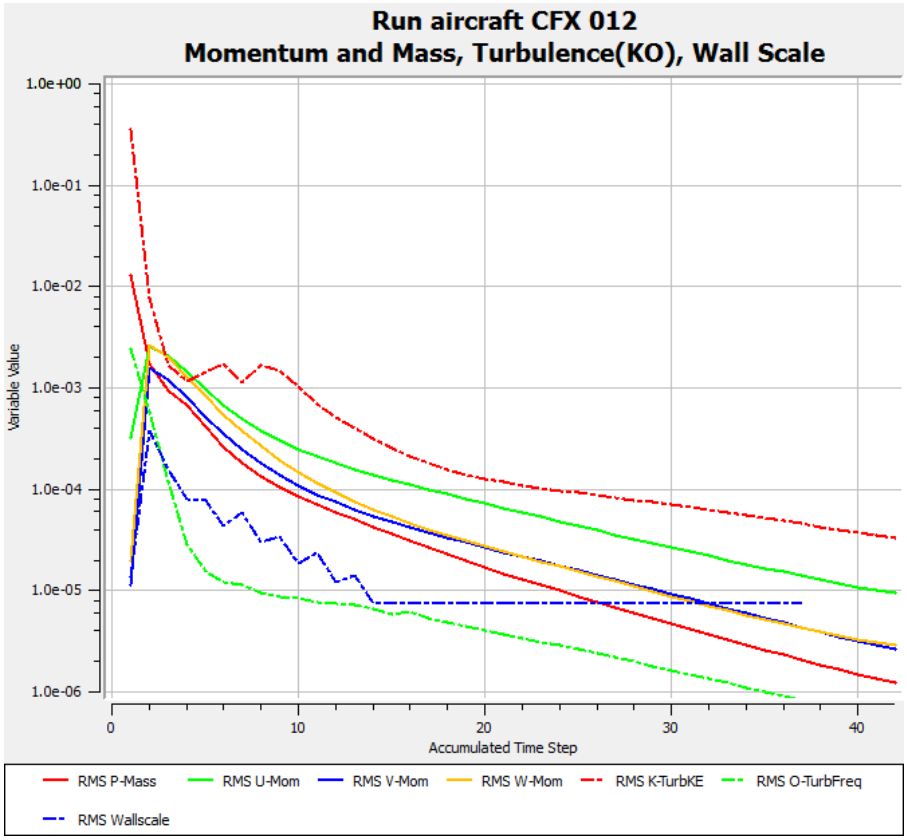

Figure 13 – The residuals history – (SST model)

Other consequence which results from the difference between SST model and k-ε model and mainly from the better resolution of the near wall area is that the convergence curve of the drag and lift coefficient are more stable. This difference is obvious from the lift coefficient curve which is in Figure 14 for the SST model and in Figure 15 for the k-ε model. From the lift coefficient curve in Figure 14 can be seen that the curve converges whereas the lift coefficient curve in Figure 15 still decreases.

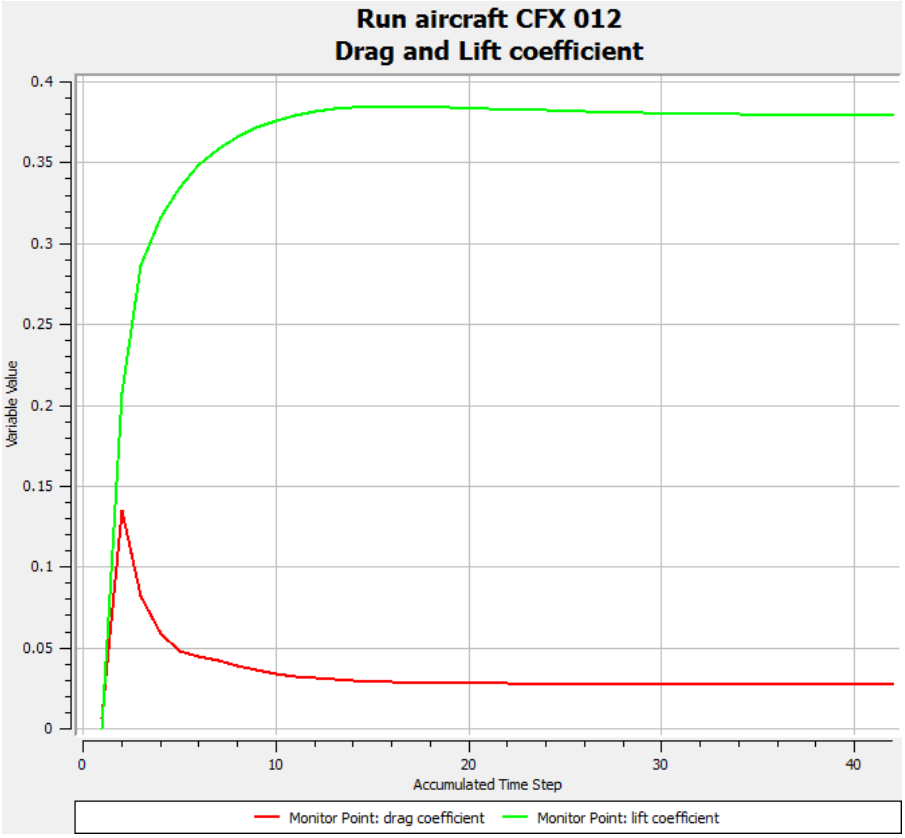

Figure 14 – The lift and drag coefficient history (SST model)

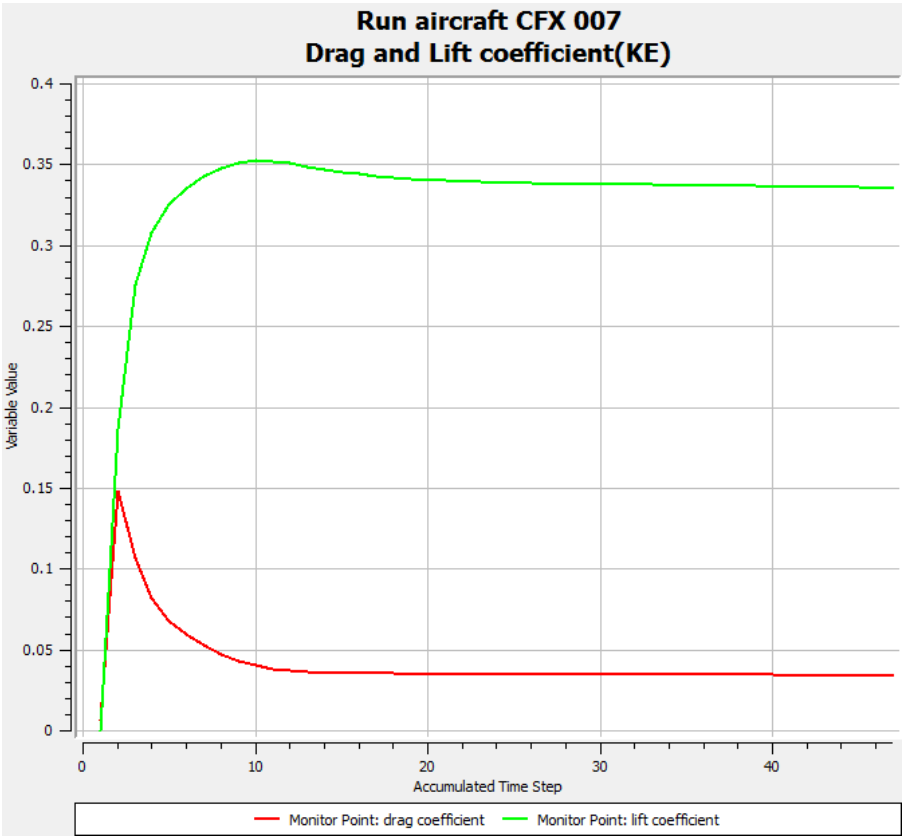

Figure 15 – The lift and drag coefficient history (k-ε model)

The convergence history of the climb and descent was more problematic. Since the quality of the mesh mainly in the vicinity of the wing was not so good to obtain non-oscillating convergence, the problems with convergence appeared and much more number of iterations must have been used to obtain required accuracy. Also the under relaxation factors were used in this phase. The influence of the under relaxation factors are shown in Figure 16 where they were applied in the 150s iteration. As the consequence of the worse mesh treatment more iteration should have been used. In the descent and climb, number of iterations needed to finish convergence with accuracy 1E-5 was over 200 iterations.

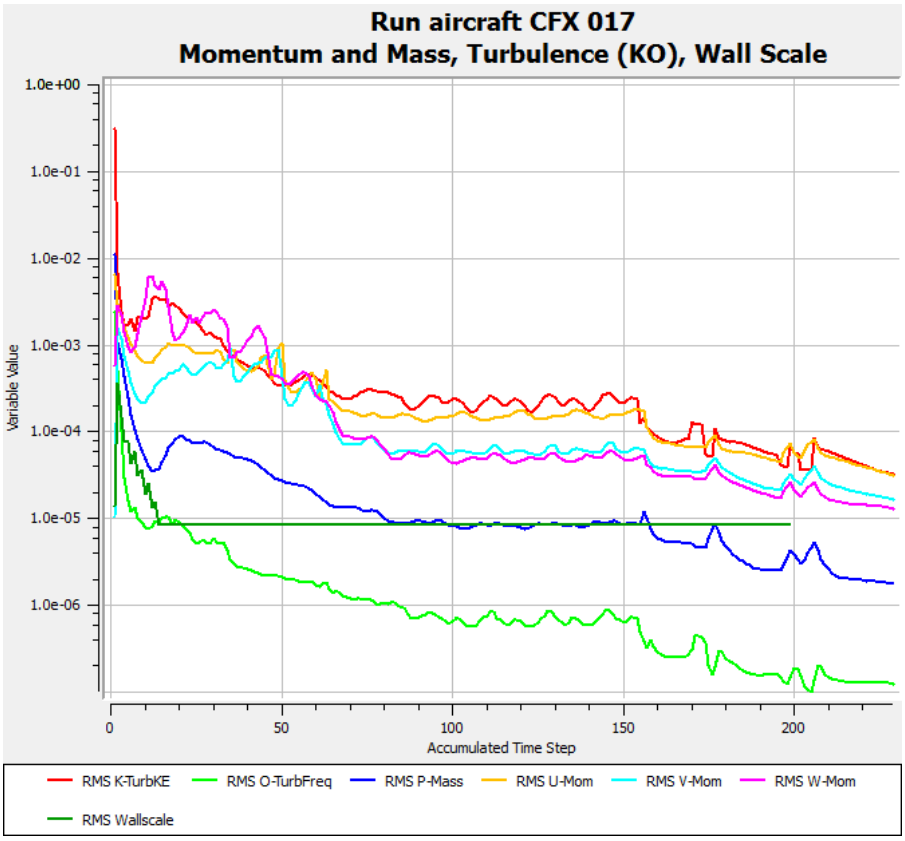

Figure 16 – The residuals history (SST model) – the descent

The history of the lift and drag coefficient, mainly of the drag coefficient, was influenced by the mesh quality. The problem was that the drag coefficient appeared with the negative sign however it is expected to be positive. In this stage the intention was to try to improve the mesh in the vicinity of the leading and trailing edge which has the most important role in evaluating drag coefficient. Unfortunately the improvement was unsuccessful so the results were strongly influenced by this issue. The explanation why this occurred is given in [6], page 362: “Pressure drag on airfoil is caused by the flow separation. For a completely attached flow over an airfoil, the pressure acting on the rear surface gives rise to a force in the forward direction which completely counteracts the pressure acting on the front surface

producing a force in the rearward direction, resulting in zero pressure drag. However, if the flow is partially separated over the rear surface, the pressure on the rear surface pushing forward will be smaller than the fully attached case, and the pressure acting on the front surface pushing backwards will not be fully counteracted, giving rise to a net pressure drag on the airfoil – the pressure drag due to flow separation. “

Since the mesh density close to the wing is not good (Fig.10) and the expected value of the drag coefficient should be according to [10] C_D=0.029, it is possible that the deviation cause the decreasing of the value of the drag coefficient under the zero. More about this kind of error can be found in [7].

This problem occurred in the climb solution as well as in the descent solution.

Since the drag and lift coefficient directly depends on the drag and lift force, the wrong value of the drag and lift force mirror the error into the coefficients. The lift and drag coefficients are calculated with formula: [6], page 24

$$C_L = \frac{L_F}{\frac{1}{2}\rho \bar{u}_{FS}^2} \tag{4.13}$$

$$C_D = \frac{D_F}{\frac{1}{2}\rho \bar{u}_{FS}^2} \tag{4.14}$$

Figure 17 shows the coefficients history in the descent. The oscillating value of the lift coefficient is caused by unstable solution of the general transport equations which appeared in Figure 16.

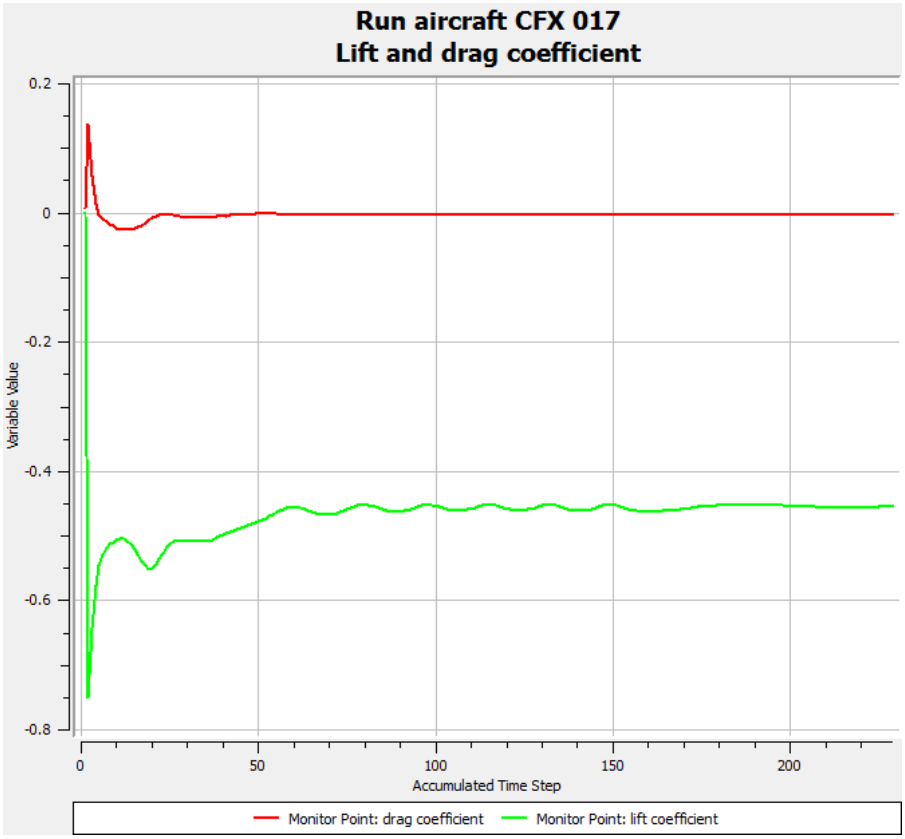

Figure 17 – The lift and drag coefficient history – the descent

4.3 Results

The y+ Value

As it was aforementioned the value of the y+ must be satisfied by the first prism. The range of the y+ is by [2] from 50 to 500. If the y+ is satisfied, the calculated results are considered to be reliable. Figure 18 depicts the y+ contour plot where the condition is nearly satisfied. Since the hardware limitation did not allow better treatment of the near wall mesh elements there are some small areas where the y+ condition is not satisfied. The areas with out of range value of the y+ are mainly in the area where the engine is connected to the wing and where the velocity is very small and it is difficult to treat these areas.

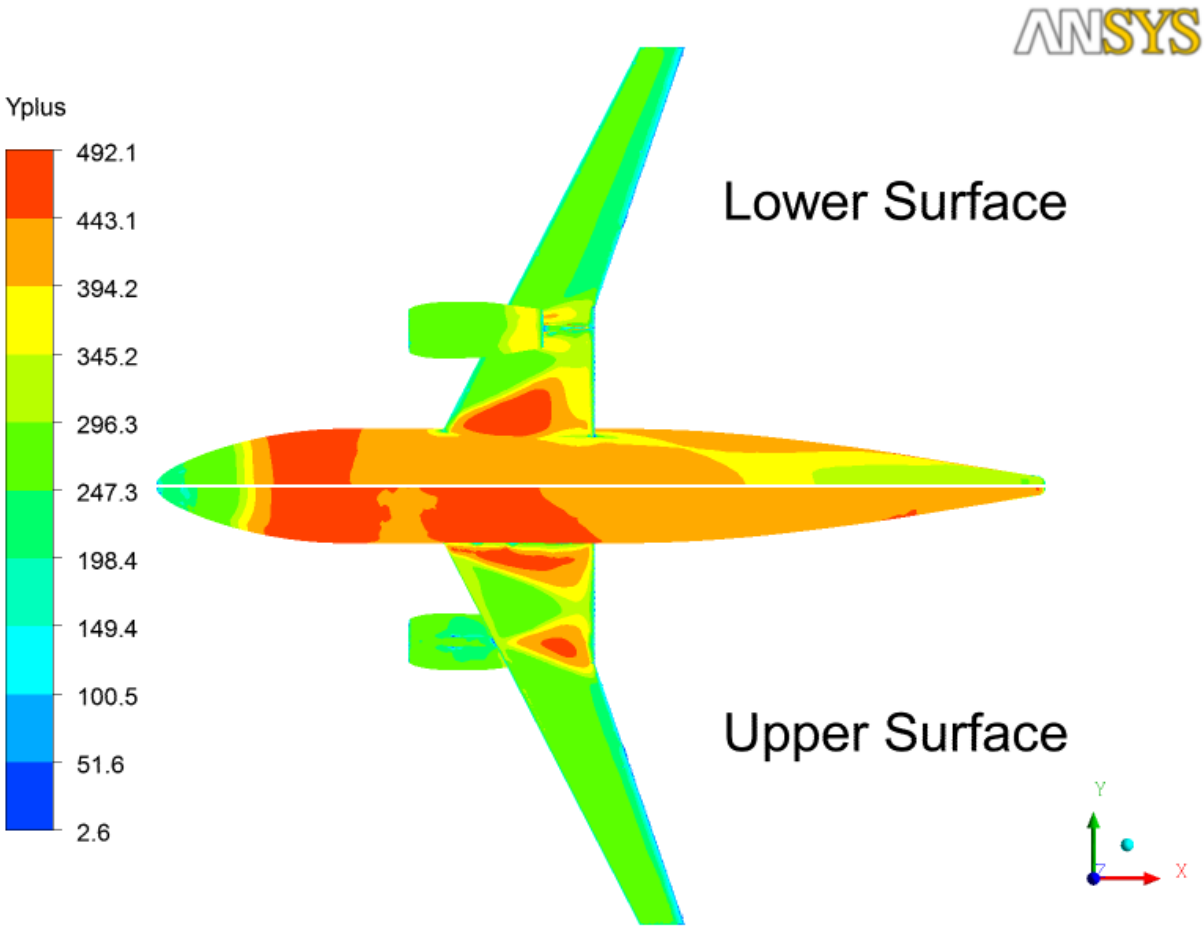

Figure 18 – The y+ value contour plot

Since the velocity profile changes with the change of the angle of attack the condition for y+ must be checked after each change of the angle of attack and the first prism height must be modified. As well as the y+ value for the cruise, the y+ value is not also satisfied at all areas of the aircraft but again in the area where the engine is connected to the wing the y+ value is lower.

Visualization Process

The visualization consists of two main features. At first, the streamlines are created in the suitable vicinity of the fuselage and wing. Moreover the vector or contour plots of the main features such as velocity and pressure are depicted. Secondly, the flow around the aircraft with its phenomena is described. The vortex is phenomenon which usually occurs in the turbulent flow and cause the major part of the drag force. The separation of the flow is other phenomenon connected with the creation of the vertices.

Two main parts of the aircraft are considered. First, the fuselage is designed to carry passengers and luggage. Second, wings are designed to produce lift and are connected with the creation of the main phenomena so the visualization is carried out mainly around the wings and on them.

4.3.1 The Description of the Flow in the Cruise

The velocity and pressure field can be described in two ways. Firstly the behaviour of the flow can be described in the direction normal to the surface and secondly in the direction along the aircraft's surface.

Since the fuselage and wing of the aircraft were set to wall, the velocity at the wall is zero and increases in the direction normal to the surface which is depicted in the detail view in Figure 19. The behaviour of the velocity should be similar to that depicted in Figure 2.

The flow around the aircraft obeys Bernoulli's equation and the conservation of the mass (Eq.2.4):

$$p + \frac{1}{2}\rho v^2 = const. \tag{6.1}$$

In Figure 19 there is a stagnation point at the top of the nose where the velocity is zero and consequently the pressure has its magnitude (Fig.20). The same is along the leading edge of the wing where the stagnation line is located. Along this line the velocity tends to zero and pressure has its magnitude to obey Bernoulli's equation.

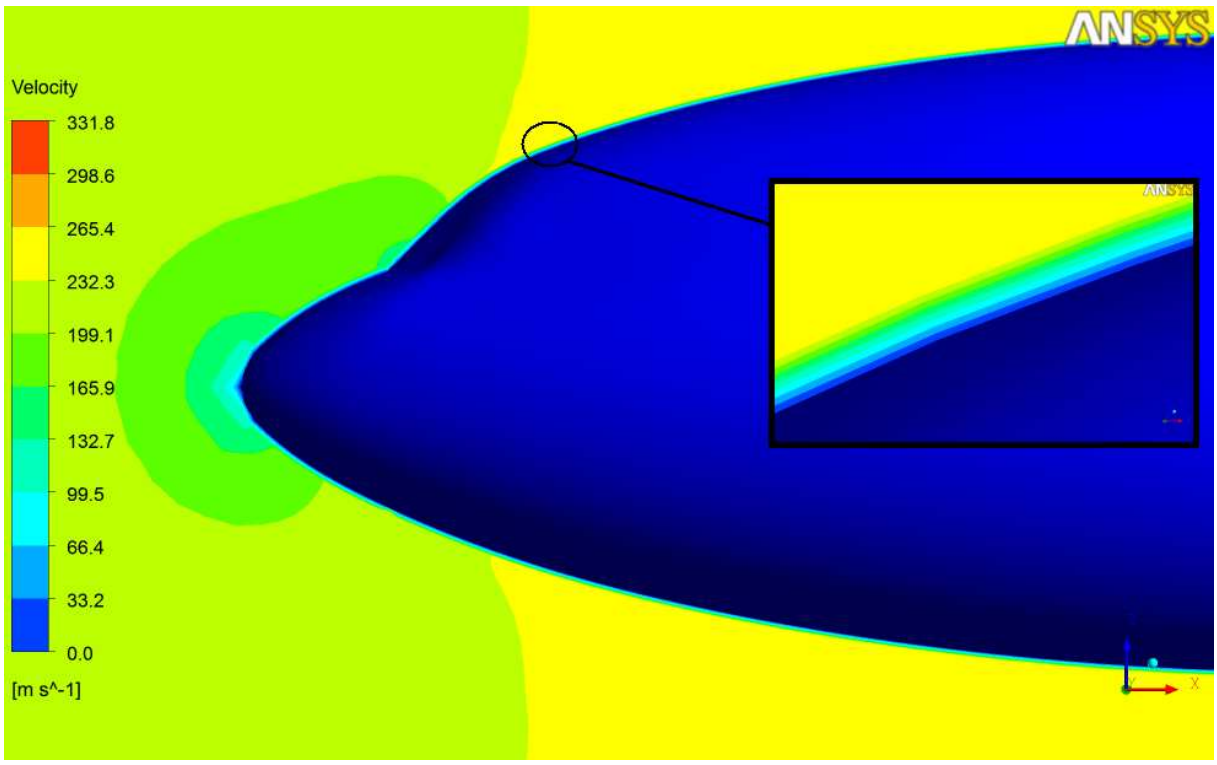

Figure 19 – The velocity contour plot in the symmetry plane with the detail of the velocity boundary layer

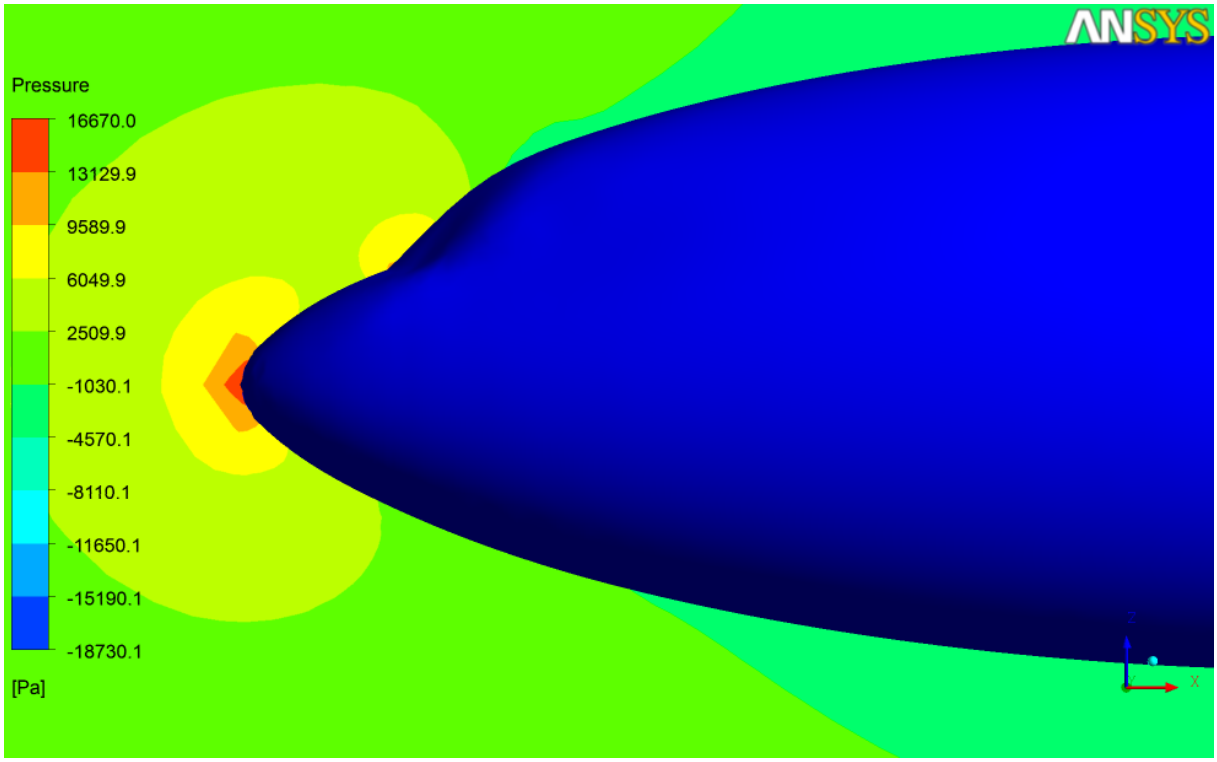

Figure 20 – The pressure contour plot in the symmetry plane

Farther along the leading edge the velocity increases (Fig.21) and pressure decreases (Fig.22). However the magnitude of the velocity on the upper surface of the wing is greater

than the velocity magnitude on the lower surface. This is due to the mass conservation along with Bernoulli's equation (Eq.6.1). Near the trailing edge the velocity goes to zero and the separation could occur. Since the wing has very good aerodynamic shape and the position of the wing in the cruise is the ideal position where usually vortices are not very significant the separation is not sufficient for the creation of the vortices.

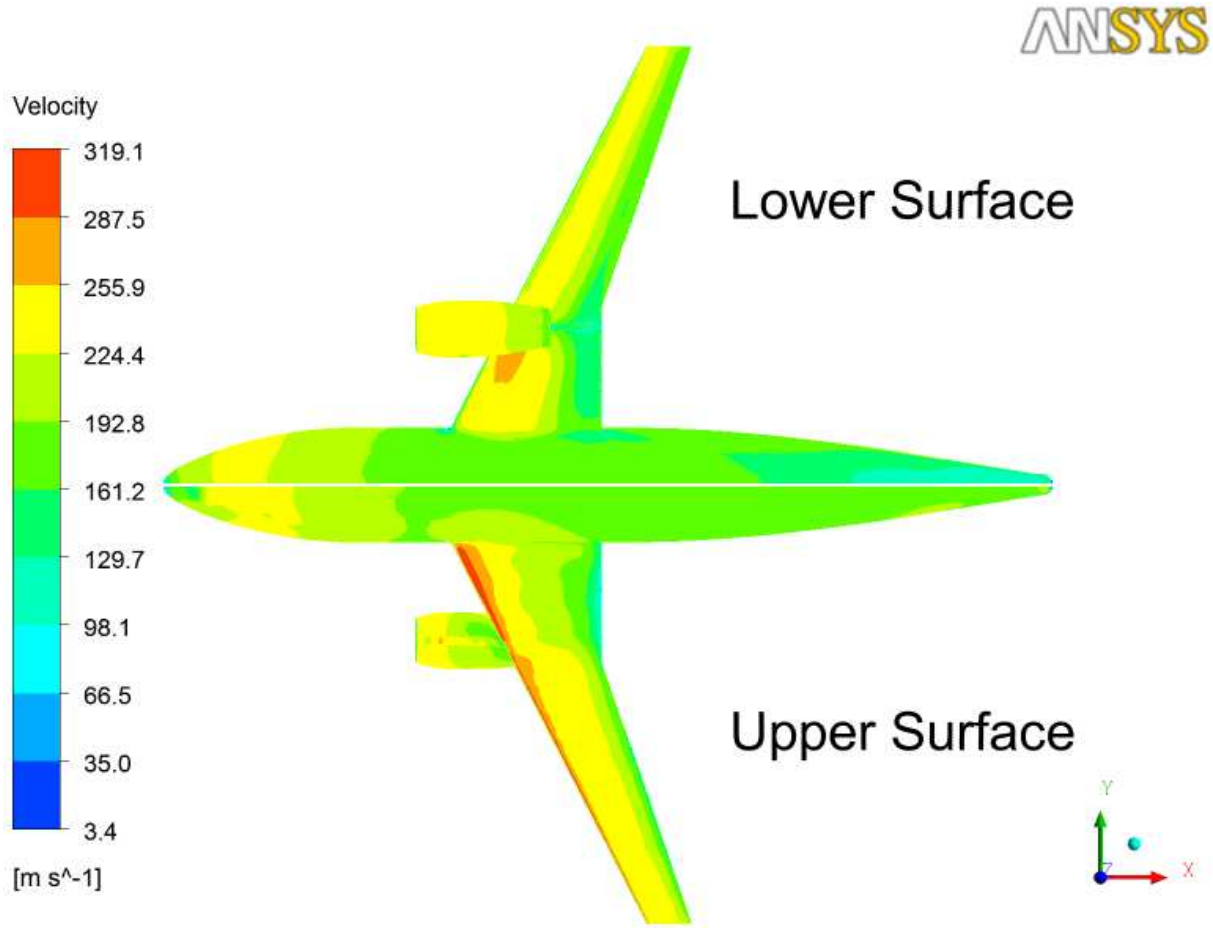

Figure 21 – The velocity contour plot – the cruise

From Figure 22 can be seen that the lift force is created on the lower surface. Since the pressure on the wing on the lower surface is greater than the pressure on the wing on the upper surface, the lift force appears. The value of the lift force depends on the pressure difference between upper and lower surface. It is necessary to generate an upward lift force which exactly balance the weight to sustain an aircraft in the air in steady flight. If the aircraft climbs, the lift force must be greater than the weight.

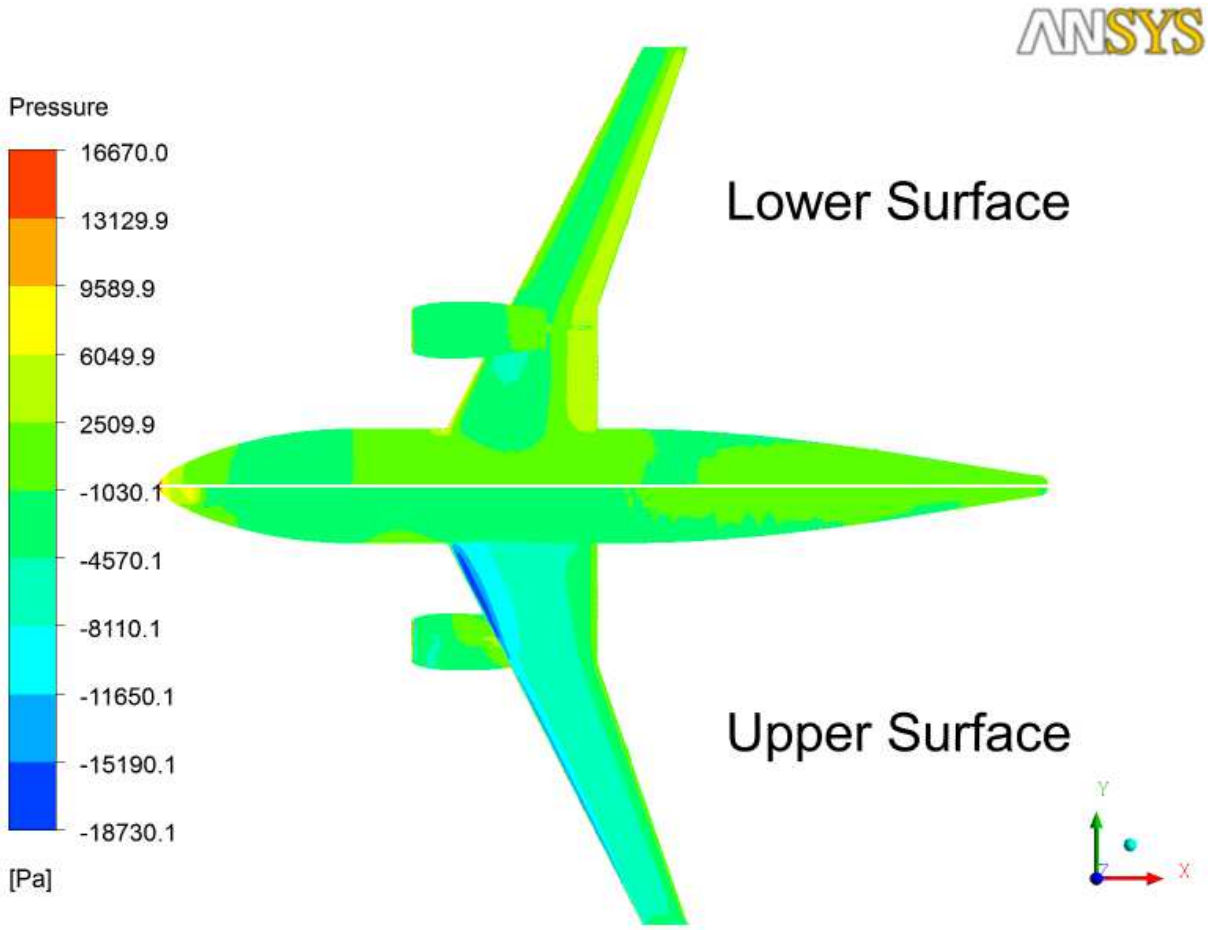

Figure 22 - The pressure contour plot - cruise

Figure 23 represents the streamlines visualization. The yellow streamlines represent limit streamlines above the wing in the order of millimetres, the red ones are six millimetres higher. The limit streamline is such a streamline which starts at the inlet then goes over the wing continuously and finally reaches the outlet.

Figure 23 shows that the shape of the streamlines is same along the wing and adjoins to the wing. However they differ near the fuselage where they are influenced by the flow around the fuselage and tend to adjoin to the fuselage. Then they go along the fuselage until the wing is reached and than adapt to the free stream. So the streamlines move smoothly over the wing and there is no flow separation of any consequence. The streamlines goes over the wing smoothly along its upper surface as well as along its lower surface. Only those are depicted which goes over its upper surface for the clarity of the picture.

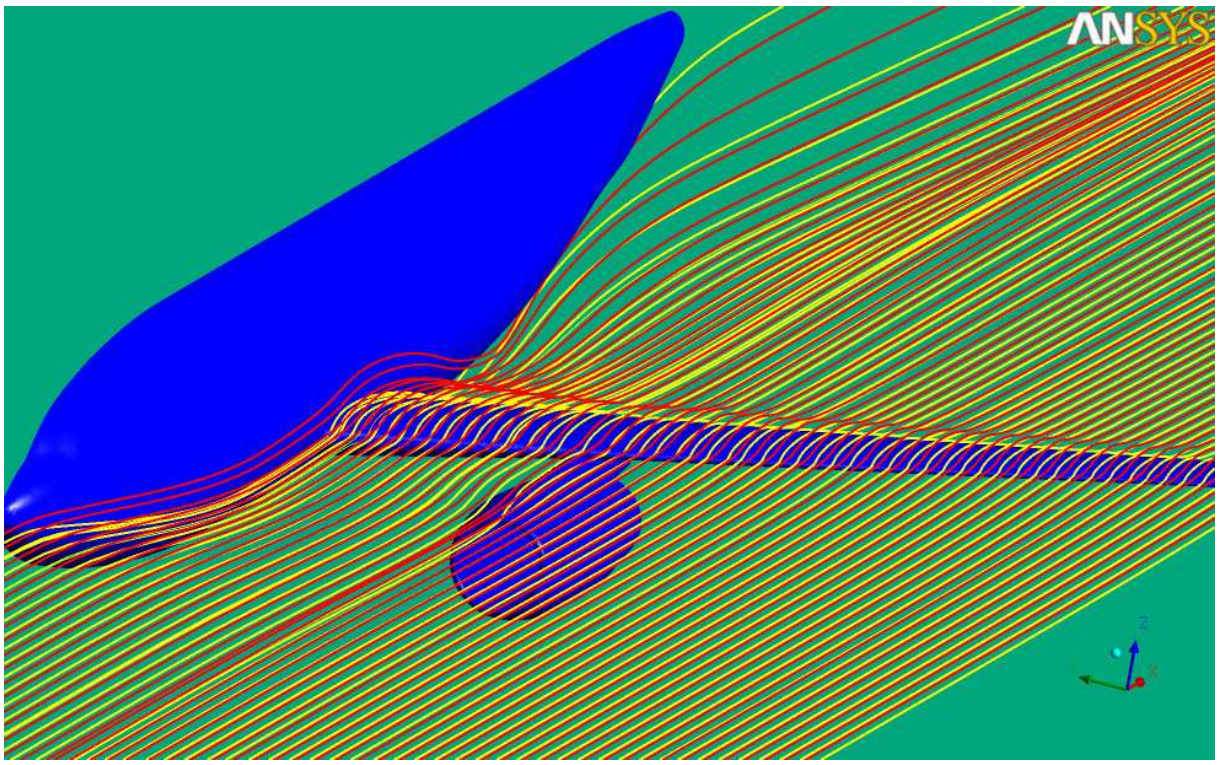

Figure 23 – The streamlines around the wing in the cruise

4.3.2 The Description of the Flow in the Climb

The most distinguishable change in the behaviour of the flow around the wing under the non-zero value of the angle of attack in comparison to the cruise (angle of attack equals zero) is that the significant vortices and other phenomena behind the wing appear.

Figure 24 shows streamlines which do not move so smoothly over the wing like it was in cruise. There are two places where the vortices are significant. The streamlines move smoothly mainly over the one part of the engine and then over the end of the wing. These places are denoted in Figure 24 by two black circles. The vortices in the other locations can be seen in Figure 24. The limit streamlines create two obvious beams. First is more compact and is created from the streamlines between the engine and fuselage. Second is created from the streamlines which hits the leading edge between engine and the end of the wing. So there can be found the cross-section area of the domain where the significant vortices can be seen on the velocity contour plots and where they can not be seen. One of such place was chosen for description of the behaviour of the flow over the wing in climb.

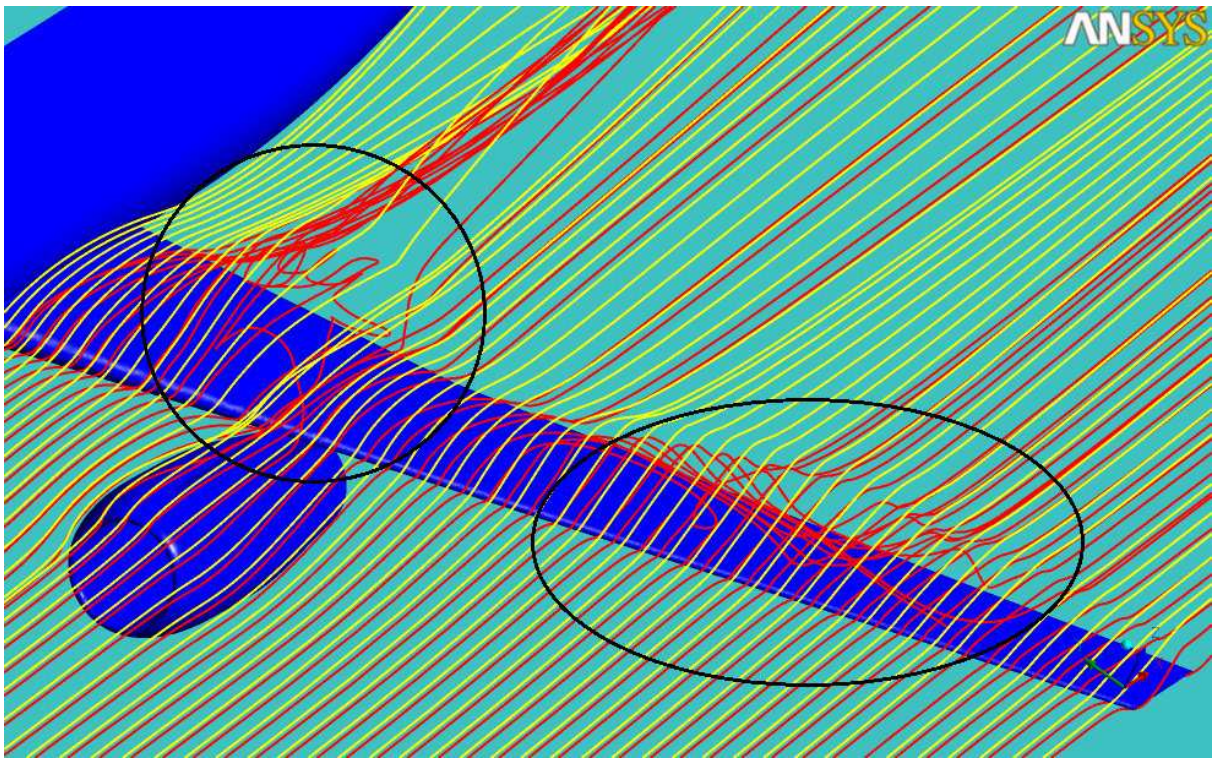

Figure 24 - The streamlines around the wing in the climb

The flow obeys Bernoulli's equation (Eq.6.1) again. Figure 25 shows that the location of the stagnation line is now just under the leading edge (on the lower surface) in comparison to the cruise. This is depicted in Figure 25 but also in Figure 26 which shows the pressure contour plot around the wing. In Figure 25 the circular area of darker blue colour which represents lower velocity tending to zero and which is a sign of the location of the stagnation point. In Figure 26 the circular dark red area depicts the place with high pressure which is in agreement with Bernoulli's equation (Eq.6.1). So in the vicinity of the leading edge the pressure is dramatically decreased. Then as the flow move farther downstream, the pressure gradually increases, reaching a value slightly above free-stream pressure at the trailing edge. This region of increasing pressure is called a region of adverse pressure gradient. By definition, an adverse pressure gradient is a region where pressure increases in the flow direction.

Farther from the leading edge to the upper surface the velocity increases. The velocity magnitude is located on the upper part of the leading edge and after the magnitude was reached it started to decrease. Once the zero velocity was reached it started to increase again. In this point the separation occurs. In case of the climb the separation is followed by formation of the vortex in the recirculation zone behind the wing. The recirculation zone in terms of pressure contour plot is depicted in Figure 26 by the green colour above the wing.

Since the area of the wing on which the air hits is bigger and the flow wake is created behind the wing than significantly greater lift force appears. Along with angle of the attack has positive value the lift force is also much greater the aircraft climbs.

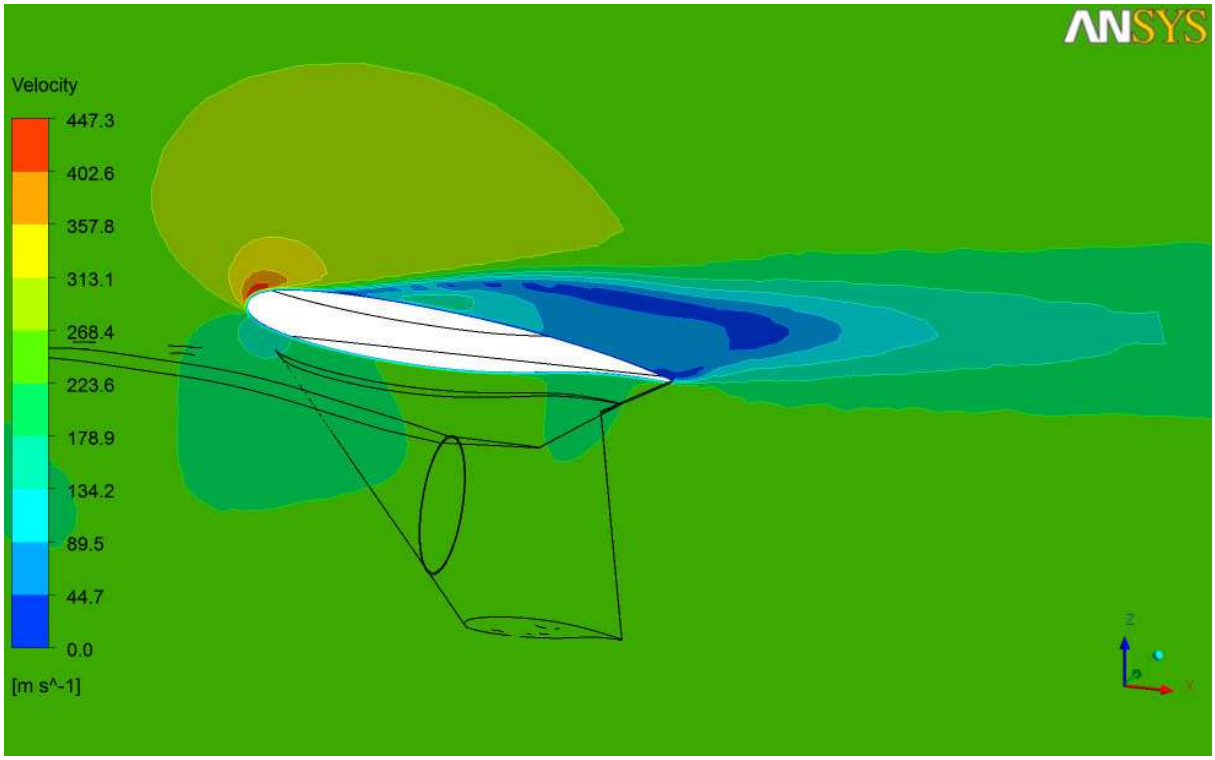

Figure 25 – The velocity contour plot around the wing – the climb

Figure 26 – The pressure contour plot around the wing – the climb

Figure 27 depicts the velocity contour plot of the aircraft in the climb. There can be seen the places where separation occurs, recirculation zones and their location along the wing. The velocity increases farther from the leading edge and if the zero velocity is reached the separation occurs. The area behind the separation place is called recirculation zone. There are two areas which fulfils this condition. There are denoted in Figure 27 by two black rectangles.

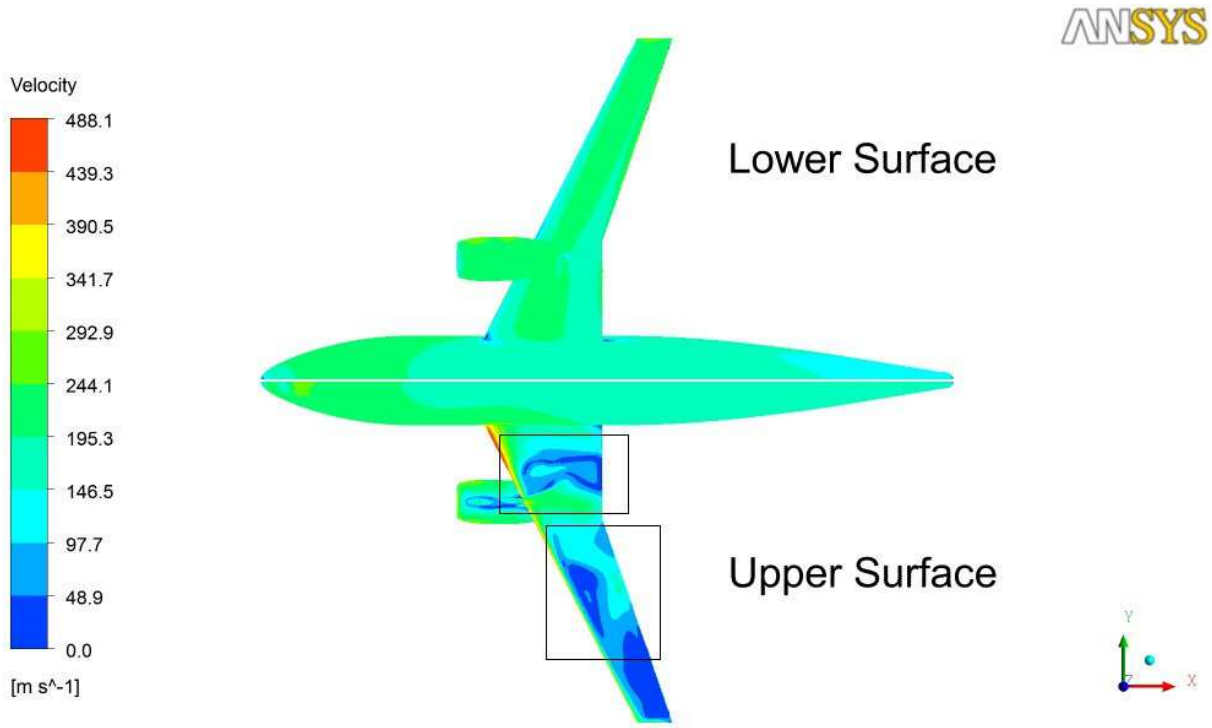

Figure 27 – The velocity contour plot – the climb

Figure 29 depicts the detail of the flow under the wing in the engine area with y-coordinate equals to -0.15m. The location of the plane used in the results part is depicted in Figure 28. In Figure 29 there is also shown velocity vector plot along with streamlines. There is shown recirculation zone in which the vortex was created and the direction by means of velocity vector plot is depicted.

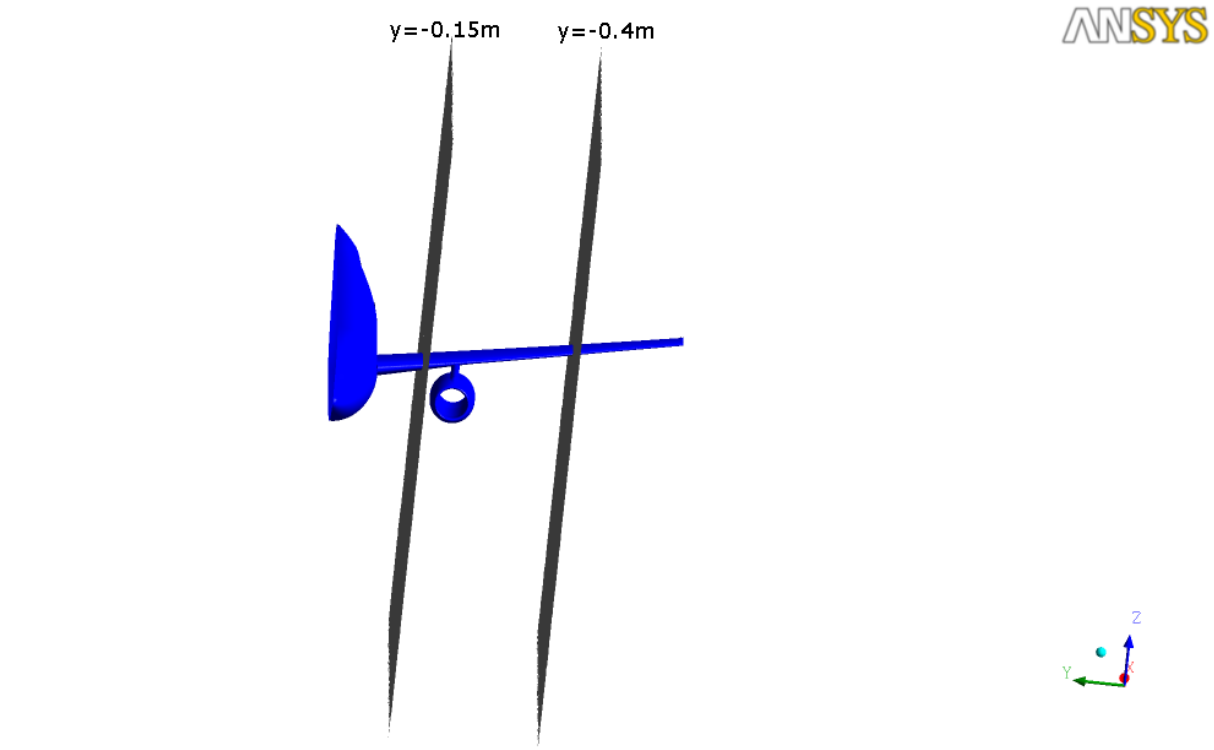

Figure 28 – The location of the planes

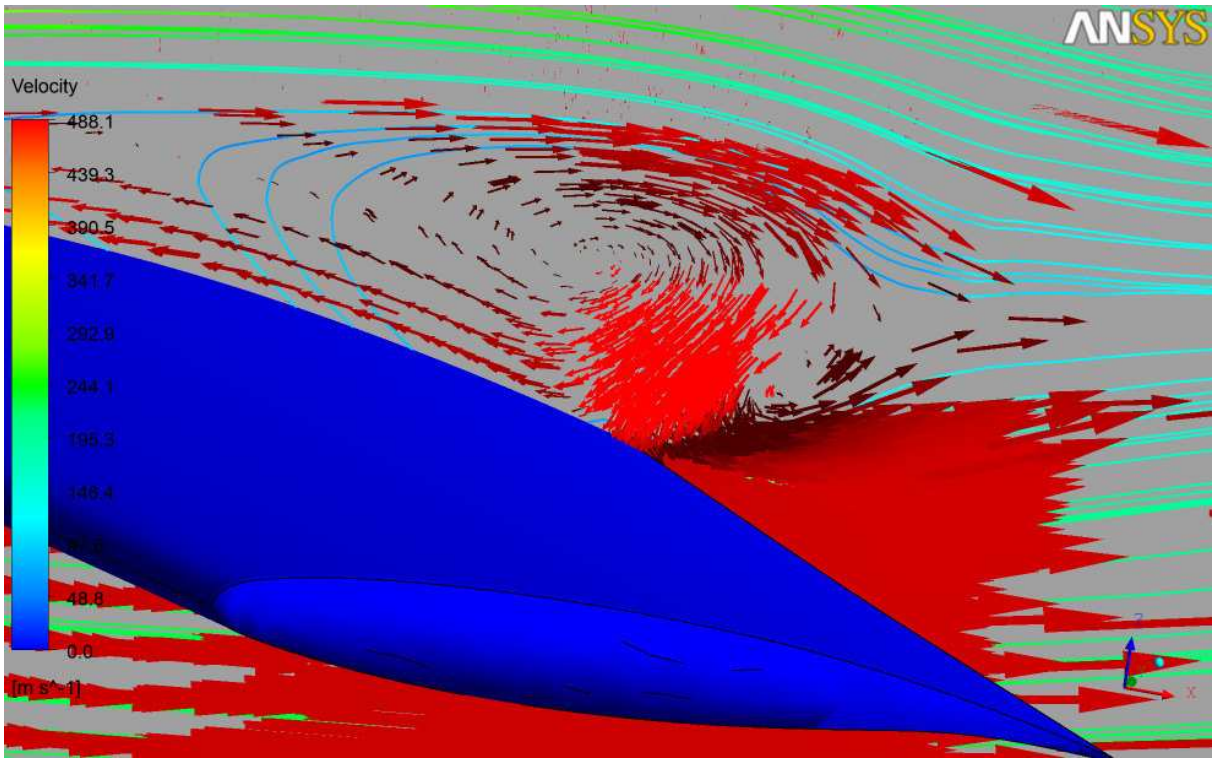

Figure 29 – The vector velocity plot along with the streamlines – the climb

4.3.3 The Description of the Flow in the Descent

It was aforementioned that more frequent phenomena are observed in the behaviour of the air flowing around the wing under the non-zero angle of attack than in comparison with cruise. The phenomena which occurs during the descent around the aircraft is similar to those which occur during the climb.

Figure 30 shows the streamlines around the lower surface of the wing. The aircraft is upside down. The limit streamlines, red ones, show how the air behaves near the surface of the wing. Other streamlines, yellow ones, are 6 millimetres lower than red and show that the behaviour of the flow located not so far from the wing is not so influenced by the vortices created under the wing. Also either streamlines show that their behaviour changed if they are in the area between the fuselage and engine or between the engine and the end of the wing.

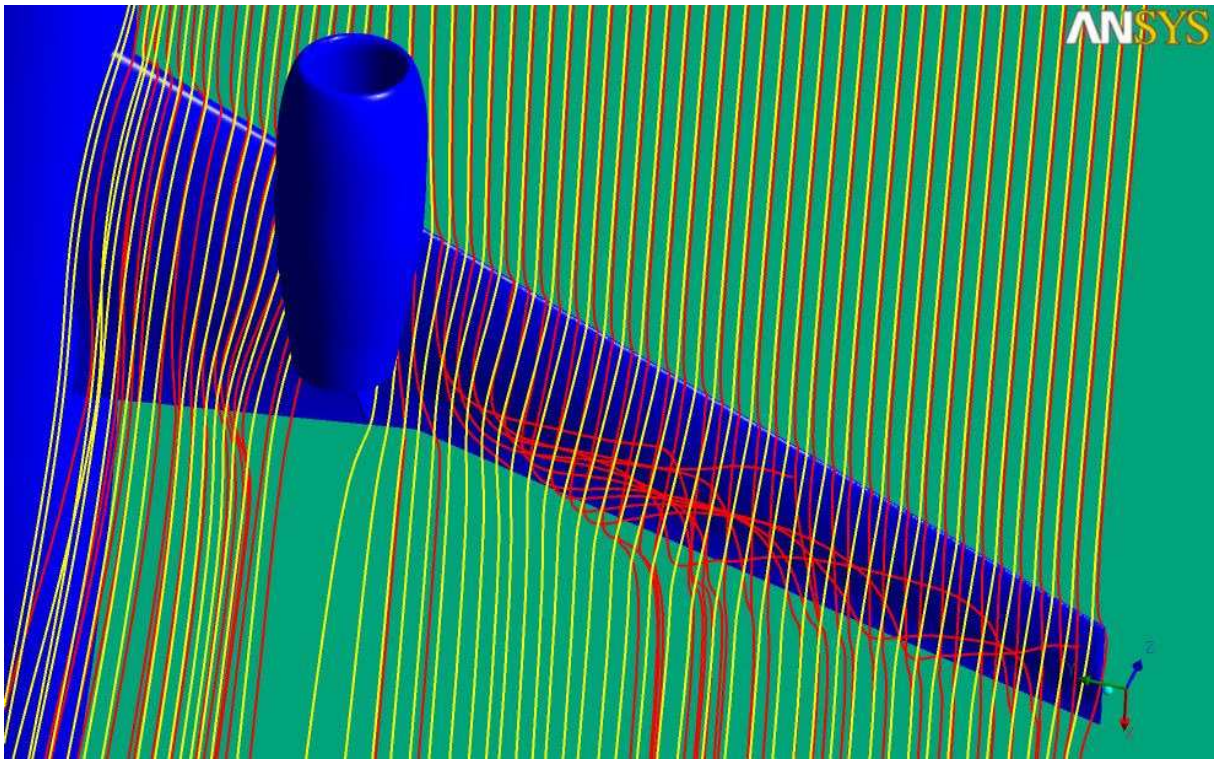

Figure 30 - The streamlines around the wing in the descent

Figure 31 depicts the velocity contour plot nearly at the end of the wing whereas Figure 32 depicts pressure contour plot in the same location. The y-coordinate of this plane is -0.3m and its location on the plane is depicted in Figure 28. The area where the stagnation line goes through can be seen in the upper part of the leading edge in both Figures, 31 and 32. The area in the upper part of the leading edge where velocity tends to zero is depicted in Figure 31

whereas in Figure 32 the stagnation point is located in the red area in the upper part of the leading edge which represents the area of the high pressure. According to the Bernoulli's equation (Eq.6.1) and mass conservation equation (Eq.2.4) and because the distance from the stagnation point to the trailing edge along the upper surface is longer than the distance along lower surface there is a place in the lower part of the leading edge where the velocity has its magnitude and than slowing down. Behind the wing the vortices are created, this time it occurs in its lower part. They are created under the same conditions stated in the climb part.

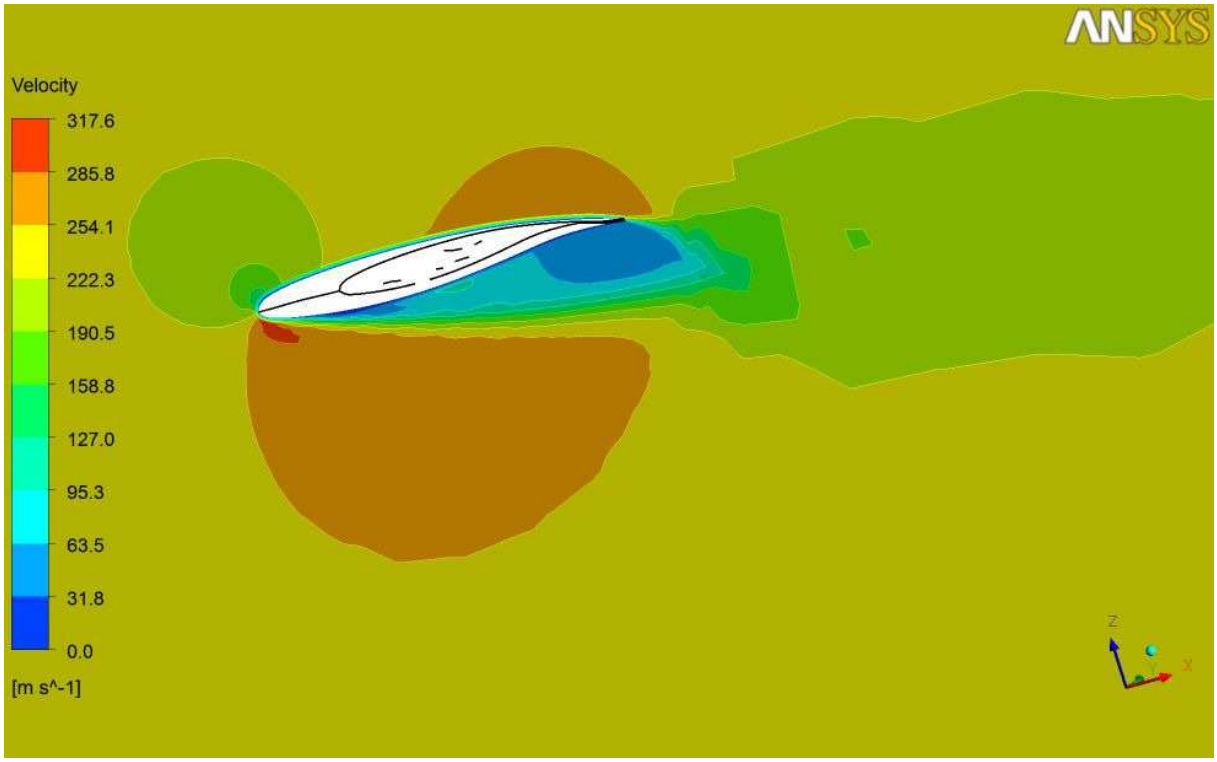

Figure 31 – The velocity contour plot – the descent

The behaviour of the pressure along the wing on its both sides corresponds to the behaviour of the velocity and obeys Bernoulli's equation. So near to the stagnation point there is the area of the highest pressure whereas in the area where the velocity has its magnitude the pressure is very low.

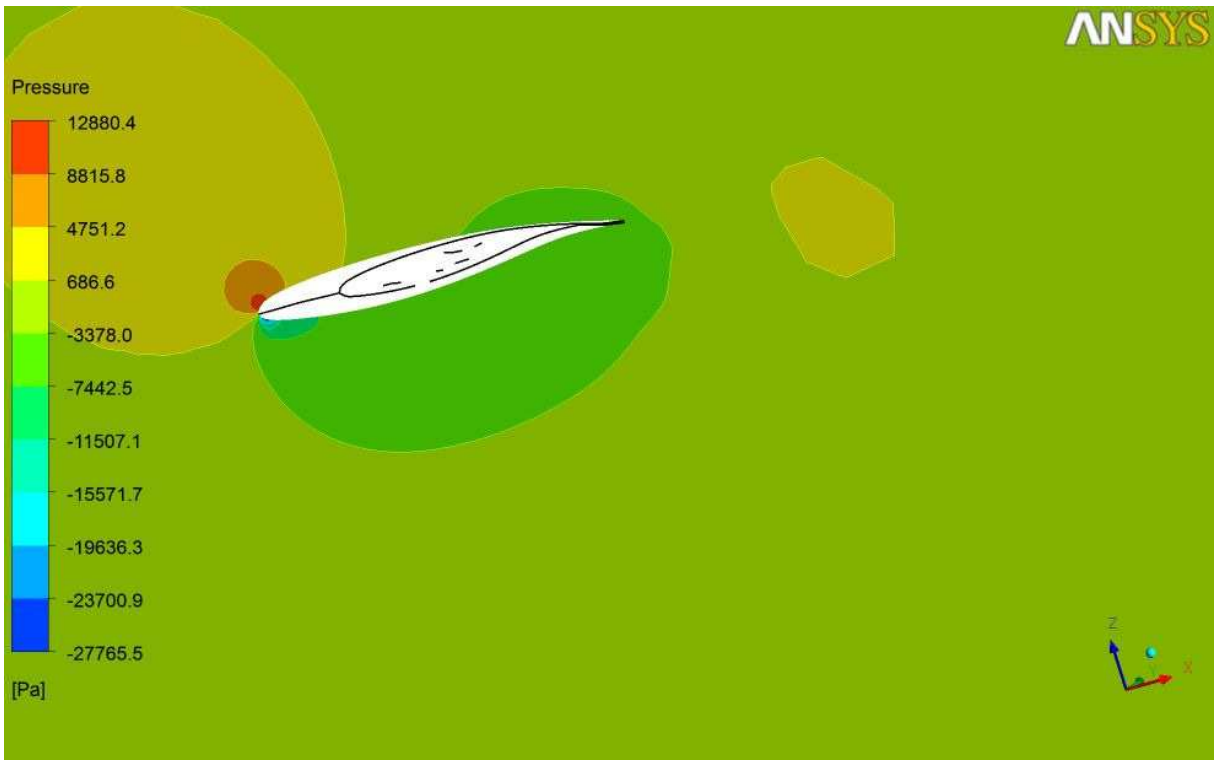

Figure 32 – The pressure contour plot – the descent

Figure 33 shows streamlines in the rear part of the wing close to the trailing edge along with the velocity vector plot.

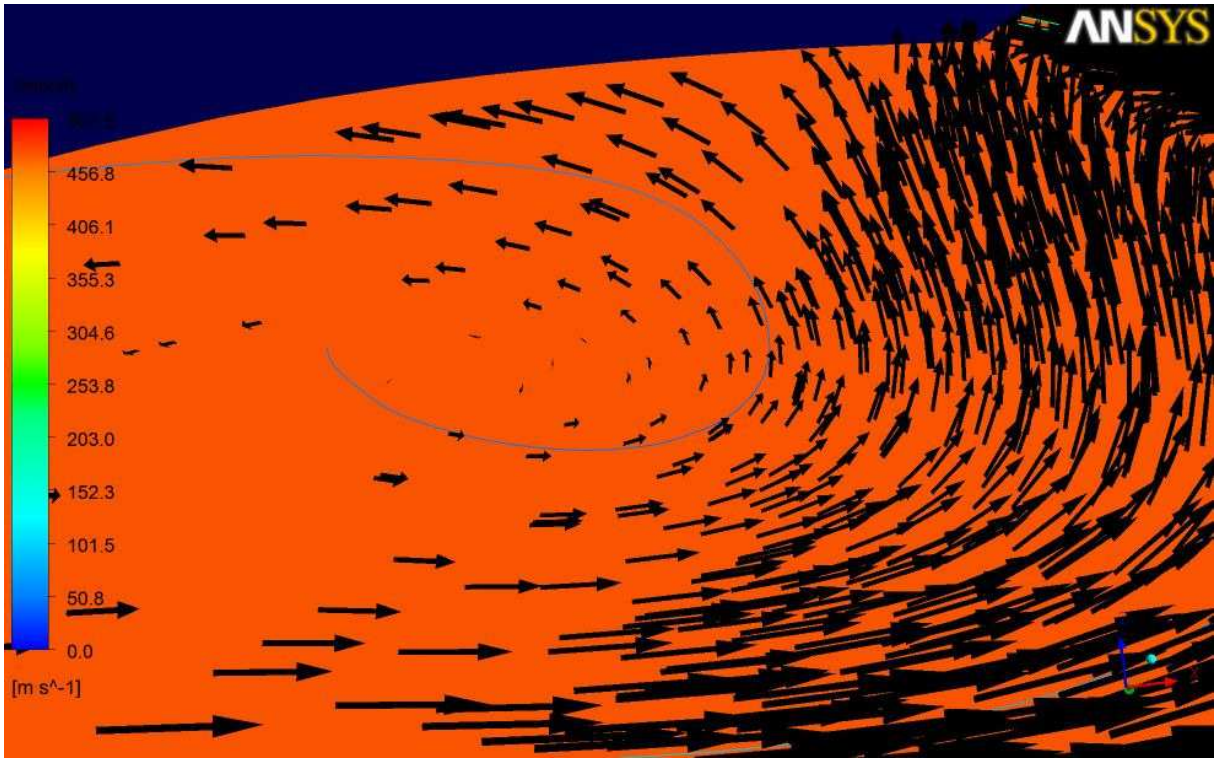

Figure 33 – The streamlines along with the vector velocity plot

Figure 34 depicts the velocity contour plot if the aircraft is in the descent. Also from this Figure can be seen separation and the regions where the recirculation zone is located. On the lower surface on the wing in Figure 34 are this regions denoted by two black rectangles.

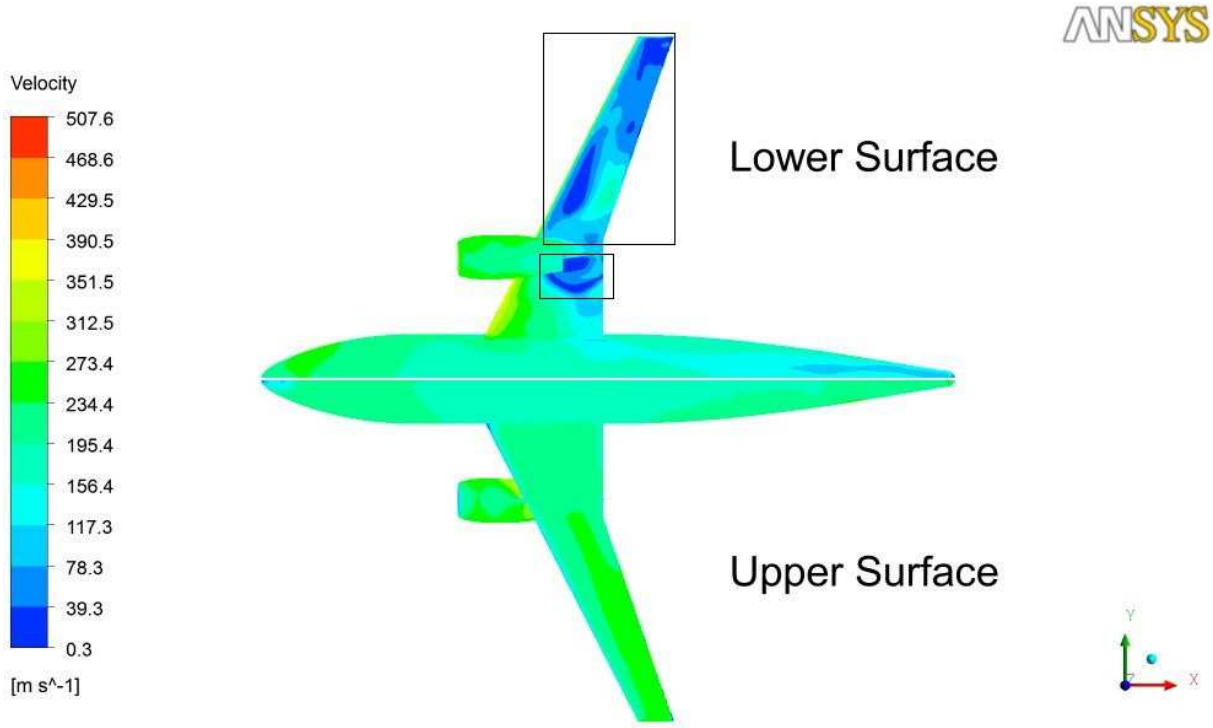

Figure 34 – The velocity contour plot – the descent

Let us turn back to the problem with the drag coefficient where the negative value appeared. Figure 35 depicts pressure contour plot of the upper surface of the wing during the descent and Figure 36 depicts the same plot of the lower surface. Only red and dark orange colour shows the location of the positive pressure whereas the rest of the colours depict the negative value of the pressure acting on the surfaces. Roughly speaking the range of the value of the red colour of the pressure according to the range of the yellow colour (but negative), the same case is for dark and light orange colour. Only green colour has higher negative value of the pressure. From these Figures one can notice that the pressure is nearly at the balance. Since value of the drag coefficient should be close to the zero, the small deviation caused by insufficient mesh density may result into the negative value of the drag coefficient. Since the pressure is in relationship with the force and the drag coefficient so if there is negative value of the pressure there is also negative value of the drag coefficient.

Figure 35 – The pressure contour plot – the upper surface

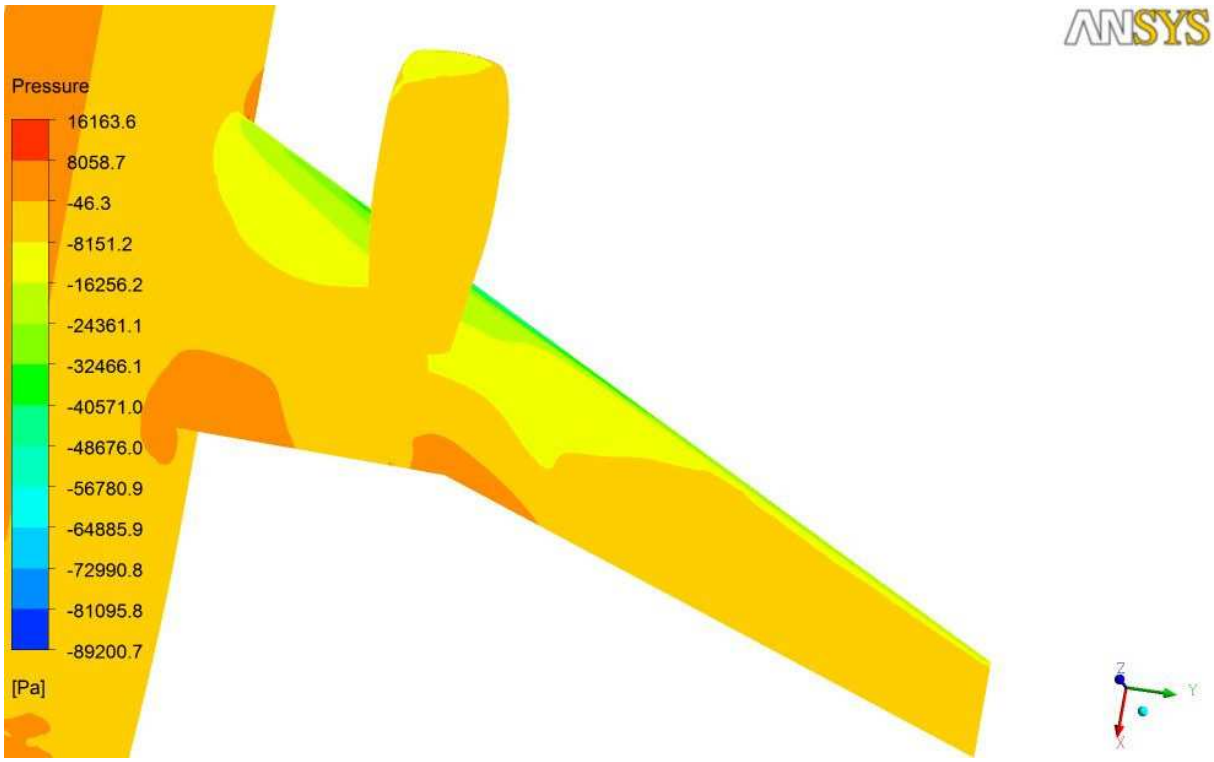

Figure 36 – The pressure contour plot – the lower surface

5 *The Improvement of the Solution and Further Calculations*

In order to improve the solution and obtain better and more accurate results more powerful computer equipment is needed. The mesh density should be refined mainly in the vicinity of the wing but also in the vicinity of the fuselage. From Figure 37 can be seen that the transition of the velocity value is not very smooth. The lower value of the lift force and subsequently the lift coefficient is also caused by the coarse mesh as well as worse distinguish of the phenomena which occur during the climb, descent but also during the cruise.

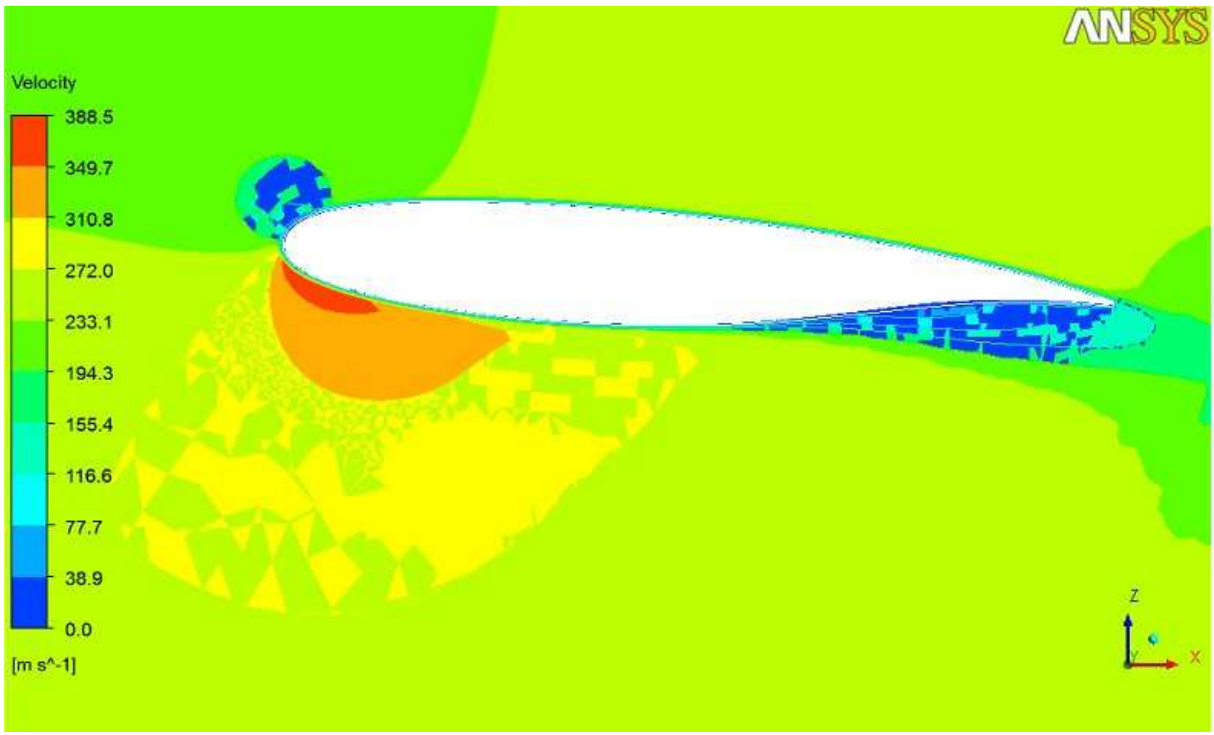

Figure 37 – The mesh quality

Although the flow around the aircraft was solved with the good accuracy there is also a possibility to put it down.

The aforementioned features of the aircraft are also limitations of the full description of the flow around the aircraft. The visualization and description of the flow only around the wing was provided but there is a place to solve the flow around the tail wings which are not part of the provided model. Furthermore, the vertical and horizontal stabilisers can be analyzed to obtain the visualization of the flow in the bend. Moreover the behaviour of the flow around the aircraft landing gear and how the properties of the flow around the whole aircraft are influenced during landing could have been modelled.

Due to lack of the more powerful computer there were neglected some issues such as the roughness of the wall. More difficult issue such as the turbulence caused by the air itself could have been taken into account.

With using other CFD software there is also possibility to choose more advanced finite differencing or finite volume schemes. In [11] there were used Roe's flux difference splitting and Spalart-Allmaras model as a turbulence equation model. With using other than common differencing scheme along with more powerful computer there can be reached better accuracy and the prediction of the flow nearly identical to the real flow.

CFD codes also enable to solve the flow of the higher Mach numbers which can be used to model the flow around supersonic aircraft where a different phenomena occurs.

6 Conclusion

The basic relationships for the description of the turbulent flow were introduced along with the relationships used in the CFD analysis. The k-ε model and SST model were used for the solution of the flow around the aircraft. Other equations which were necessary i.e., mass conservation and momentum equation were also introduced.

The models intended for the CFD analysis are not always suitable for it without modifications. The provided model of the aircraft was analyzed in symmetry boundary condition because of its time and costs requirements. The model of the aircraft was printed into the block which created the fluid domain.

The flow domain was discretized using approx. 9 million of 3D elements as tetrahedral, pyramids or wedges. The inflated layers were implemented around the surface of the aircraft to distinguish the flow behaviour in the buffer layer. The key part of the analysis was the suitable mesh within the hardware limitation. The upper and lower surface of the wing were treated sufficiently to provide realistic results whereas the leading and trailing edge suffered from the hardware limitation and it was not possible to treat there edges sufficiently. The boundary conditions were applied to the dicretized fluid domain. The inlet, outlet, wall, symmetry and opening boundary conditions were set using pressure and velocity values. The outlet boundary condition could not be used in the simulation of the climb and descent because of its intention only for the flow predominantly directed out of the domain. However, the fluid is also directed into the domain in the simulation of the climb and descent, so the outlet boundary condition was changed into the opening boundary condition.

The simulation was performed for 3 different angles of attack. Then the streamlines and pressure and velocity field were solved and visualized. The separation region and vortex creation was found out behind the wing. The reliability of the solution was controlled through the y+ value which was satisfied on the major part of the surface of the aircraft. Also the zero velocity at the surface was satisfied.

The model is also suitable for simulating of the pressure fields, velocity profiles and for the judging of the influence of the other parts of the aircraft, i.e., landing gear on the fluid flow. The simulation of the flow around the solid body is important not only for the solution of the aerodynamics and aircrafts, but also in the car industry, power engineering or to design

the cooling of the electromotors. The fluid flow problem can be also accompanied by the stress analysis i.e., multifield problem, which involve the influence of the temperature, deformation or forces, all in one task.

7 Software and References

Software

[1] Ansys 12.0

[2] Microsoft Office

[3] Gimp – raster graphics editor

References

[1] HUGHES, William F.; BRIGHTON, John A. *Fluid dynamics*. Third edition. [s.l.] : McGraw Hill, 1999. viii, 391 p. ISBN 0-07-031118-8.

[2] VERSTEEG, H.K.; MALALASEKERA, W. *An introduction to computational fluid dynamics : The finite volume method*. [s.l.] : Pearson Education Limited, 2007. xiii, 503 p. ISBN 978-0-13-127498-3.

[3] DOUGLAS, John F.; GASIOREK, Janusz M.; SWAFFIELD, John A. *Fluid Mechanics : Fourth Edition*. [s.l.] : Pearson Education, 2001. xxvi, 911 p. ISBN 0-582-41476-8.

[4] BERTIN, John J.; CUMMINGS, Russell M. *Aerodynamics for engineers*. Fifth Edition. [s.l.] : Pearson International Edition, 2009. 752 p. ISBN 978-0-13-2355-21-6.

[5] *Www.boeing.com* [online]. 2010 [cit. 2010-04-20]. Available on WWW: www.boeing.com.

[6] ANDERSON, John D., Jr. *Fundamentals of Aerodynamics*. [s.l.] : McGraw-Hill, 2007. xxiv, 1008 p. ISBN 978-0-07-295046-5.

[7] FERZIGER, J.H.; PERIĆ, M. *Computational Methods for Fluid Dynamics*. 3rd edition. [s.l.] : Springer, 2002. vii, 423 p. ISBN 3-540-42074-6.

[8] *Www.ansys.com* [online]. 2010 [cit. 2010-04-20]. Available on WWW: www.ansys.com.

[9] ANSYS® Academic Research, Release 12.0, Help System, ANSYS, Inc.

[10] RIVERS, Melissa B.; HUNTER, Craig A.; GATLIN, Gregory M. Support System Effects on the DLR-F6 Transport Configuration in the National Transonic Facility . In *4th AIAA CFD Drag Prediction Workshop*. NASA Langley Research Center, Hampton, VA 23681 : [s.n.], 24.6.2009. 20 p.

[11] UTYUZHNIKOV, S.V: Generalized wall functions and their application for simulation of turbulent flows. In *International journal for numerical methods in fluids*. Department of Power; Propulsion & Aerospace Engineering; School of Engineering; Cran˙eld University; Cran˙eld; MK43 0AL; U.K. : Wiley InterScience, 7.1.2005. 6 p.